Paleoceanography and Paleoclimatology

RESEARCH ARTICLE
10.1029/2025PA005100

Approaching the Miocene Climatic Optimum in Patagonia (Southern Argentina): Temperature Seasonality and a Potential Role for the Opening Drake Passage

Linda C. Ivany[1], Claudia J. del Río[2], Maximiliano J. Alvarez[2], R. Paul Acosta[3], Kyger C. Lohmann[4], and M. Sol Raigemborn[5,6]

[1]Department of Earth and Environmental Sciences, Syracuse University, Syracuse, NY, USA, [2]CONICET- Museo Argentino de Ciencias Naturales, CABA, Argentina, [3]Department of Atmospheric, Oceanic, and Earth Sciences, George Mason University, Fairfax, VA, USA, [4]Department of Earth and Environmental Sciences, University of Michigan, Ann Arbor, MI, USA, [5]CONICET–UNLP, Centro de Investigaciones Geológicas, La Plata, Argentina, [6]Facultad de Ciencias Naturales y Museo (UNLP), La Plata, Argentina

Abstract The Miocene Epoch (23.03–5.33 Ma) is receiving increased attention because estimated pCO_2 and its associated warmth is comparable to projections over the next century. Well-constrained sea-surface temperatures in the tropics and northern latitudes express amplified warming during the Miocene Climatic Optimum (MCO; 16.9–14.7 Ma), yet data from the Southern hemisphere are few, especially in the mid-high south Atlantic, and proxies appear to suggest only moderate warming. Here, we present seasonally resolved oxygen isotope data from fossil marine bivalves in the Early Miocene (Burdigalian) Monte León Formation of southern Patagonia, Argentina, and explore their implications for Miocene paleoclimate. Paleoclimate simulations from the Miocene isotope enabled Earth System Model (iCESM1.2) allow for proxy-model comparison. Mean annual paleotemperatures increase from ~15°C to ~20°C between ~19.3–17.5 Ma, consistent with model predictions at 400 and 560 ppm CO_2, respectively. Using a recently reported isotopically positive ocean, calculated paleotemperatures are 4°C warmer still, more akin to the warmth documented in the early-mid Miocene northern hemisphere. Both reinforce mid-high-latitude warmth in the approach to the MCO, but the second well exceeds model-predicted temperatures, even at higher pCO_2. Seasonal range increases upsection from ~3.5°C to ~6.4°C, with more warming in the summer, potentially reflecting an increase in the influence of a seasonally oscillating Malvinas current on the Patagonian coast associated with an increasingly open Drake Passage. The fact that paleoSSTs are substantially warmer than those in the study area today (6–10°C), despite only moderately elevated estimated pCO_2, merits further attention.

Plain Language Summary Understanding the response of global temperatures to changes in the amount of CO_2 in the atmosphere is integral to the study of Earth's climate system in the past and critical for predicting the conditions we face in the near future. The Miocene Epoch (23–5 million years ago) receives particular attention because estimated CO_2 is comparable to today. During the Miocene Climatic Optimum (MCO, ~17 to 15 million years ago), temperatures rose significantly, but we know little about what happened in the Southern Hemisphere, where data are scarce. We analyzed shells of fossil marine mollusks from Patagonia (southern Argentina) from just before the MCO to estimate ancient ocean temperatures and compare them with predictions from an ocean-atmosphere climate model. We find that ocean temperatures increased from ~15°C to 20°C, consistent with inferences drawn from the fossil record of Patagonia and matching model predictions for CO_2 rising from 400 ppm (near today's atmosphere) to 560 ppm. Seasonal range in temperatures also increased, possibly linked to changing circulation through the Drake Passage (between South America and Antarctica). Remarkably, even with only moderately elevated CO_2, ocean temperatures in Miocene Patagonia were much higher than today (6–10°C)—something that warrants further study.

Key Points:

- Early Miocene paleoclimate proxy data from the southern hemisphere are sparse
- $\delta^{18}O$ of fossil bivalves from southern Patagonia show warming and increasing seasonality in the lead-up to the Miocene Climatic Optimum
- Proxy data agree with iCESM1.2 models of 400–560 ppm CO_2; minor mismatch opens the potential for influence by changes in the Drake Passage

Correspondence to:
L. C. Ivany,
lcivany@syr.edu

Citation:
Ivany, L. C., del Río, C. J., Alvarez, M. J., Acosta, R. P., Lohmann, K. C., & Raigemborn, M. S. (2025). Approaching the Miocene Climatic Optimum in Patagonia (southern Argentina): Temperature seasonality and a potential role for the opening Drake Passage. *Paleoceanography and Paleoclimatology*, *40*, e2025PA005100. https://doi.org/10.1029/2025PA005100

Received 13 JAN 2025
Accepted 5 MAY 2025

Author Contributions:
Conceptualization: Linda C. Ivany, Claudia J. del Río
Data curation: Linda C. Ivany, Maximiliano J. Alvarez, R. Paul Acosta
Formal analysis: Linda C. Ivany, Claudia J. del Río, Maximiliano J. Alvarez, R. Paul Acosta, Kyger C. Lohmann
Funding acquisition: Claudia J. del Río, Maximiliano J. Alvarez, M. Sol Raigemborn
Investigation: Linda C. Ivany, Claudia J. del Río, Maximiliano J. Alvarez, Kyger C. Lohmann, M. Sol Raigemborn
Methodology: Linda C. Ivany, Claudia J. del Río, Maximiliano J. Alvarez, R. Paul Acosta, Kyger C. Lohmann

1. Introduction

How global mean annual temperature (MAT) and the distribution of temperature over Earth's surface vary in response to changes in pCO_2 is important for predicting future conditions on our anthropogenically warming planet. The Miocene Epoch is receiving increased attention from the climate community because estimated pCO_2 is comparable to that forecast over the next century ($CenCO_2PIP$ et al., 2023) and proxy data suggest warm conditions relative to today (Steinthorsdottir et al., 2021). Proxies for pCO_2 and temperature generally covary

Project administration: Linda C. Ivany, Claudia J. del Río
Resources: Claudia J. del Río, Maximiliano J. Alvarez, M. Sol Raigemborn
Visualization: R. Paul Acosta
Writing – original draft: Linda C. Ivany, Claudia J. del Río
Writing – review & editing: Linda C. Ivany, Claudia J. del Río, Maximiliano J. Alvarez, R. Paul Acosta, Kyger C. Lohmann, M. Sol Raigemborn

through the Cenozoic, including simultaneous increases during the Miocene Climatic Optimum (MCO) between 16.75 and 14.5 Ma, perhaps initiated by the Columbia River flood basalts (Kasbohm and Schoene, 2018) and augmented by high rates of sea-floor production (Herbert et al., 2022), reinforcing the first-order control of pCO2 on global temperature over geologic time (CenCO_2PIP et al., 2023). The Early Miocene, however, is emblematic of an interval of comparatively stable temperatures (late Oligocene to Middle Miocene) that interrupts the long-term cooling trend of the Cenozoic (Burls et al., 2021; Westerhold et al., 2020) despite evidence for persistently falling pCO_2 (CenCO_2PIP et al., 2023). Tectonically driven opening and closing of ocean gateways and associated changes in circulation can overprint the climate response to CO_2 forcing, both regionally and globally (Lunt et al., 2016), and these are thought to play a role during this interval.

Global climate models offer powerful tools with which to understand the response of the climate system to changes in both pCO_2 and paleogeography, but model-based predictions and estimates of equilibrium climate sensitivity must be informed by proxy data from the rock record to ensure that they adequately capture the most fundamental elements of past climates—global mean temperature and the meridional temperature gradient (Lunt et al., 2024; Tierney et al., 2020). Zonal heterogeneity combined with sparse and geographically patchy data (e.g., Douglas et al., 2014) can complicate efforts to constrain these parameters. During the Early Miocene, proxy data on sea-surface temperatures (SSTs) are few and heavily skewed toward the tropics and northern latitudes; those from the mid and high southern latitudes are especially sparse and confined almost entirely to the eastern hemisphere (Burls et al., 2021).

Here, we present marine paleotemperatures for the Early Miocene (Burdigalian) from SE Patagonia (Argentina), a region heretofore virtually devoid of proxy data and proximal to the widening Drake Passage, a gateway long thought to be important in the evolution of Cenozoic temperatures (e.g., Kennett, 1977) and potentially influenced by changes in Antarctic ice-sheet volume (Gasson et al., 2016; Hoem et al., 2023). Patagonia boasts a rich stratigraphic record spanning much of the Miocene and containing assemblages of marine mollusks, therefore offering great potential for paleoclimate inference. Del Río (1990, 2021) used the compositions of mollusk faunas to infer warm-temperate SSTs in the mid-high latitudes of Patagonia during the Early Miocene—cooler than the climatic optima of the middle Eocene and the MCO but warmer than the cool-temperate waters that characterize coastal settings in the region today. We build on that work using stable oxygen isotope analysis of mollusk shell carbonate to provide quantitative estimates of paleotemperature that can be compared directly with proxy data from other regions and with climate model output to help clarify the circumstances of Miocene warmth. Stable oxygen isotope data from marine mollusk fossils can fill spatio-temporal gaps in deep-sea core coverage, as shells from open ocean-facing shelves like these can yield data that compare well to adjacent oceanic SSTs (Judd et al., 2020). In addition, because they grow by accretion over a number of years, data from sequentially sampled shells provide constraints not only on MAT but also on seasonal temperature extremes—difficult or impossible to obtain from other proxy systems but routinely generated by dynamical climate models and hence useful for proxy-model comparisons (Ivany and Judd, 2022). The Miocene Patagonian shelf section and its mollusk fossils are thus strategically positioned to offer much-needed insight on high-southern-latitude paleotemperatures in a key region (adjacent to a major opening gateway), during an important transitional time in Earth history (the lead-up to the MCO).

We integrate proxy results with predictions from an isotope-enabled, coupled climate model for the Miocene. Proxy-model agreement in this poorly constrained part of the world will lend confidence to our understanding of the climate system on a warmer planet, while disagreements offer opportunities to further refine models and explore the origins of spatial heterogeneity in proxy data. We find that MAT values are largely consistent with model predictions and warm through time, in keeping with expectations of increasing pCO_2 toward the MCO. The upper part of the section, however, is warmer and more seasonal than can be accommodated by the model, suggesting the potential added influence of changing circulation patterns brought about by the late stages of the opening of Drake Passage.

2. Geologic Setting

The Austral—Magallanes Basin in southernmost Patagonia is a foreland basin initiated by subduction and Andean compression during the Cretaceous. Superimposed on tectonically mediated subsidence and migration of the basin depocenter to the east, the basin records a number of flooding intervals over the course of the Cenozoic. One of the most extensive transgressions, the Leonense transgression, took place in the late Oligocene to Early

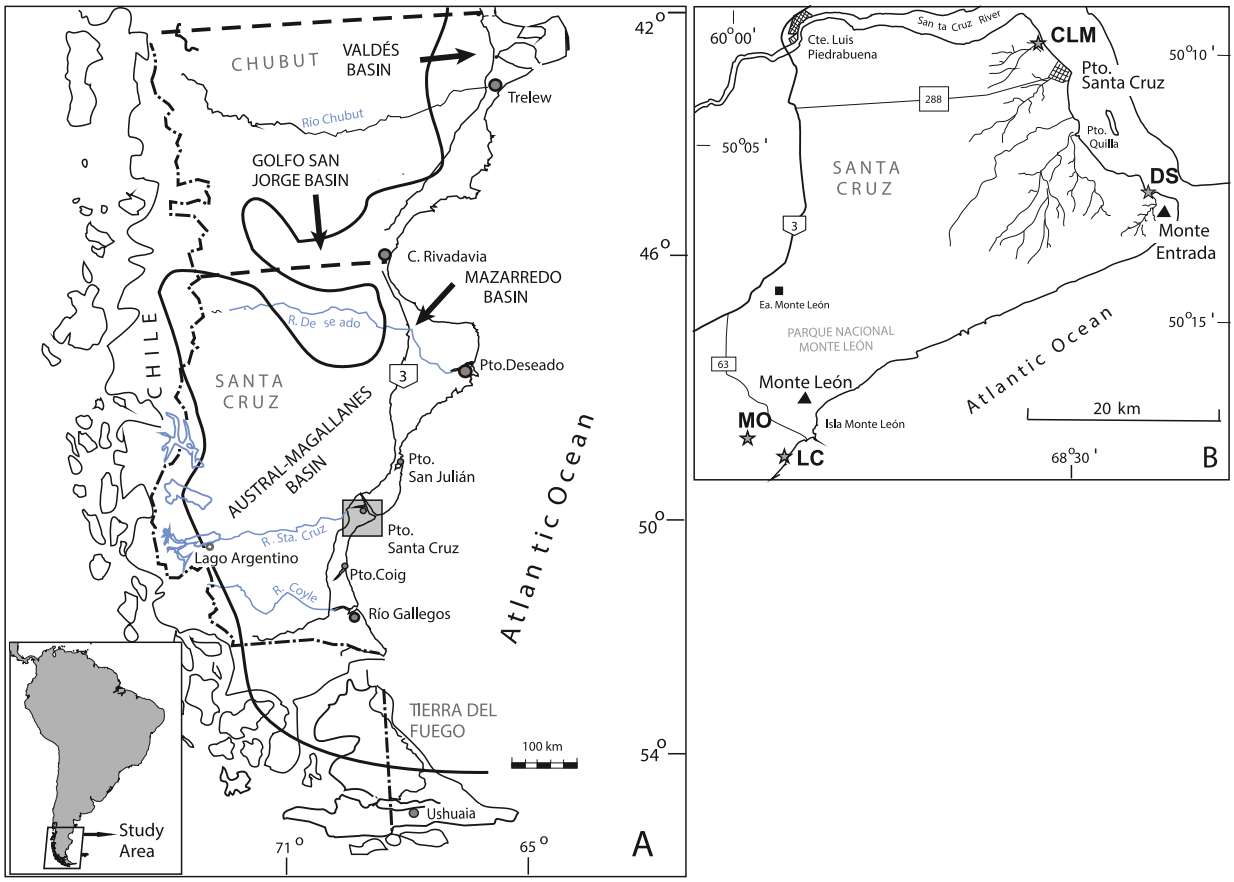

Figure 1. (a) Location of Patagonian basins during the Burdigalian (modified from del Río et al., 2022). Study area is in the shaded box; location of published data from Lago Argentino (see text) in gray open circle. (b) Inset showing locations of studied lithostratigraphic sections: CM, Cañadón Los Misioneros; DS, Darwin Section; LC-MO, Las Cuevas-Monte Observación.

Miocene, with maximum flooding between 20 and 19 Ma that reached from the Atlantic up to the eastern front of the Andes (Parras and Cuitiño, 2021). Subsequent compression associated with initial subduction of the Chilean Ridge (Dávila et al., 2018) led to uplift, exhumation, and the transition to the overlying continental deposits of the Santa Cruz Formation in the study region.

In the Austral—Magallanes Basin, the Leonense transgression is recorded by the deposition of shallow marine sediments of the Monte León Formation (MLF) (Bertels, 1970) in the east, the Estancia 25 de Mayo (formerly Centinela Formation; Cuitiño & Scasso, 2010) and El Chacay formations (Chiesa & Camacho, 1995) in the western sector, and the Carmen Silva Formation (Codignotto & Malumián, 1981) exposed in the southern sector of the basin. In the San Jorge Basin to the north, flooding is represented by the lower part of the Chenque Formation (Bellosi, 1990), and in the Mazarredo Basin to the NE by the Mazarredo Formation (del Río et al., 2022) (Figures 1a and 2). Uncertainties over age control for and correlation among these units have been resolved by a series of studies over the last decade largely using strontium isotope chronostratigraphy on fossil mollusks and $^{40}Ar/^{39}Ar$ and U-Pb age dates on intercalated volcanic deposits (summarized by del Río et al., 2022; Parras and Cuitiño, 2021).

The MLF is a 200 m thick transgressive-regressive succession that crops out along the Atlantic coast from Puerto Coyle (Coig) northwards to Puerto San Julián (Figure 1), where its basal contact with the underlying San Julián Formation (Bertels, 1970) is exposed. $^{87}Sr/^{86}Sr$ chronostratigraphy constrains deposition to between 22.12 Ma and 17.8 Ma (Parras et al., 2012), and detailed lithological and paleoenvironmental descriptions are provided by Parras and Griffin (2009), Parras and Cuitiño (2018) and Parras et al. (2020). The formation is comprised of the lower Monte Entrada Member, deposited in inner shelf to deltaic environments, and the upper Monte Observación Member deposited by a prograding deltaic system with tidal influence (Parras and Cuitiño, 2018). While minor

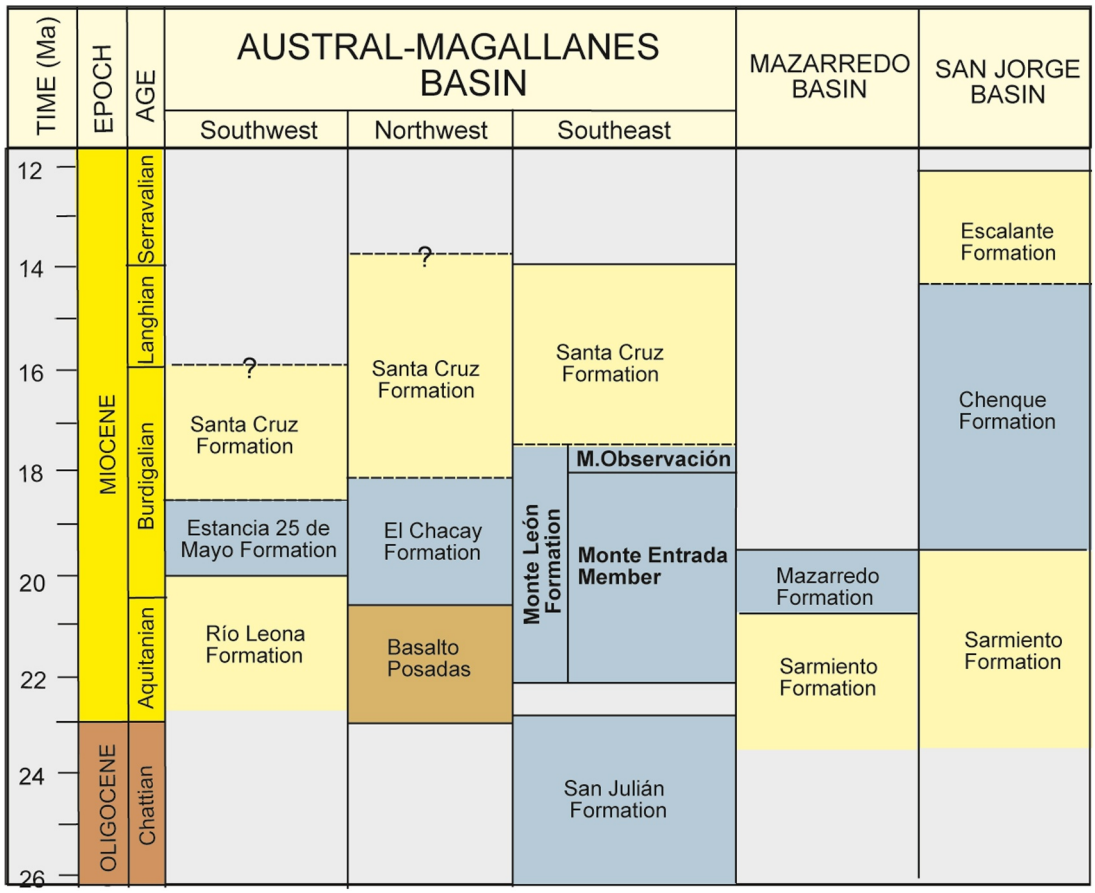

Figure 2. Correlation stratigraphic chart for all units discussed in the text. Units in bold are those from which the present data come.

disconformities are locally present in association with storm beds or channel migration in shallower facies, the unit overall reflects a single large depositional cycle of transgression and regression, without intervening sequence boundaries to suggest major hiatuses in deposition (Parras and Cuitiño, 2018). The section grades upwards into the continental Santa Cruz Formation, dated in its base at ∼17.8 Ma in the study area but as old as 19 Ma farther west, in the Andean foothills (Perkins et al., 2012).

The Monte Entrada Member is composed of intercalated yellow, gray and white tuffaceous siltstones and claystones containing numerous fossiliferous lenses overlain by tuffaceous siltstones and fine-grained sandstones with abundant concretions, large trace fossils (*Thalassinoides* sp.), and thin fossiliferous beds. The upper part of the unit is unfossiliferous mudstone and fine-grained sandstone. The Monte Entrada Member is remarkable for its unique, abundant, usually well-preserved and highly diverse molluscan fauna, including also fossil echinoids and crabs. The mollusks are dominated by ostreids, pectinids and arcoids and were among the first taxa collected by Charles Darwin in South America (Darwin, 1846), described by Sowerby (1846) and later included in the global revision of the Tertiary mollusks of Patagonia carried out by Ihering (1907). More recently, the most abundant groups have been the subject of detailed revisions, including the bivalved veneroids (Alvarez et al., 2020; del Río, 1997), pectinids (del Río, 1995, 2004a, 2006; Santelli and del Río, 2019a, 2019b), and arcoids (del Río and Camacho, 1998) and the gastropod volutids (del Río and Martínez, 2006), muricids (Griffin and Pastorino, 2005) and naticids (Griffin and Pastorino, 2013).

The Monte Observación Member is comprised of red, yellow and ochre, massive or laminated tuffaceous mudstones, fine to medium-grained sandstones, and massive or cross-stratified, coarse-grained sandstones. Intercalated fossiliferous beds are frequent and usually represented by autochthonous assemblages of the oyster *Crassostrea hatcheri* or parautochthonous, low diversity molluscan associations.

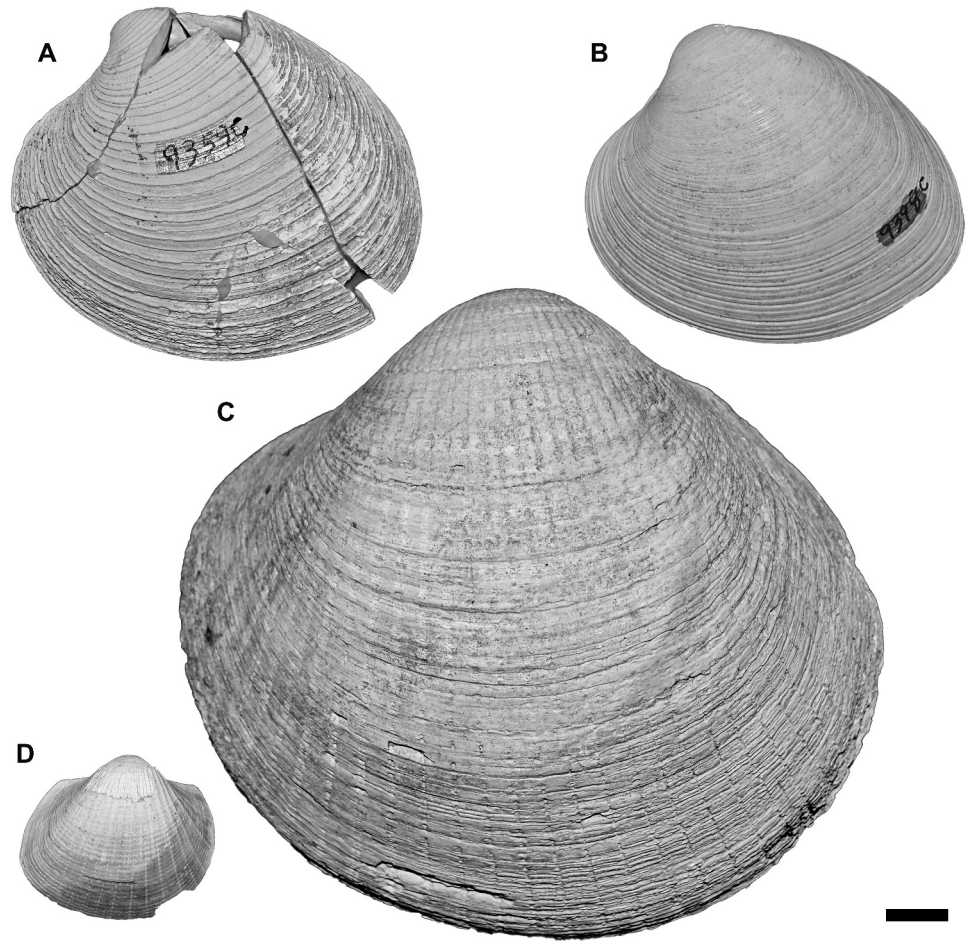

Figure 3. Studied material from Monte León Formation, Santa Cruz, Argentina. (a) *Retrotapes striatolamellatus*, CPBA 9359C, Darwin Section (DS2). (b), *Austrocallista iheringi*, CPBA 9398C, Las Cuevas (LC). (c) *Glycymerita cuevensis*, CPBA 16619, Monte Observación (MO). (d) *Cucullaea alta*, CPBA 16605, Darwin Section (DS1). Scale bar = 10 mm.

Taphonomy of the unit overall suggests variable sedimentation rates associated with episodic storm deposition in an otherwise low-energy setting. Storm-generated concentrations of shells were subsequently overprinted by burrowing infauna to varying degrees. Mollusk assemblages do not appear to be mixed or transported from outside their local habitat (Pineda-Salgado et al., 2022 and our field observations), so in situ winnowing of fines during storms, without physical transport, likely produced the concentrations of shells in this formation.

3. Material and Methods

3.1. Fossil Material

Fossils of the MLF come from outcrops located in the Parque Nacional Monte León (Santa Cruz Province) between the mouth of the Santa Cruz River and the area of Las Cuevas-Monte Observación (Figure 1b). Four species of aragonitic, infaunal, marine bivalves were selected for stable isotope paleothermometry: the arcoids *Cucullaea alta* (Sowerby) and *Glycymerita cuevensis* (Ihering), and the venerids *Austrocallista iheringi* (Cossmann) and *Retrotapes striatolamellatus* (Ihering) (Figure 3). Two of these genera are extinct - the endemic *Austrocallista* Cossmann and the cosmopolitan *Glycymerita* Finlay and Marwick; and two are extant - the paleoaustral *Cucullaea* Lamarck maintains a relict distribution in the Indian and western Pacific Oceans (Buick, 2009; Nicol, 1950), and the endemic *Retrotapes* del Río is still extant in the region. Shells were sectioned and polished to reveal internal growth banding for comparison to external growth lines on the shell surface. Specimens used for the analyses below are archived in the (Colección de Paleontologia de la Universidad de

Buenos Aires; acronym CPBA) and the Museo Argentino de Ciencias Naturales (Colección Nacional de Paleoinvertebrados; acronym MACN-Pi).

3.2. Stratigraphy

Fossils were collected from three lithological sections, two situated on the right bank of the Santa Cruz River close to its mouth (Darwin Section and Cañadón Los Misioneros), and the other (Las Cuevas-Monte Observación) 47 km south from the mouth of the river on the South Atlantic coast (Figures 1b and 4). We discuss them below in stratigraphic order moving upsection, as correlated in Figure 4.

Darwin section (50° 07′ 51.82″S; 68° 23′ 58.88″W) is situated at the cliffs between Monte Entrada and the port of Punta Quilla. In this area, exposures extend over 4.4 km of coastline and material analyzed comes from the following horizons:

DS 1: Material collected from this bed (*Cucullaea alta*) comes from fossiliferous lenses placed at 4 m above sea level (masl) and dated at 19.27 Ma by Parras et al. (2012). Faunal composition is laterally variable; dominant taxa are *Cucullaea alta* and *Turritella ambulacrum* Sowerby, followed by scarse *Reticulochlamys zinsmeisteri* del Río, *Jorgechlamys juliana* (Ihering), *Iheringinucula crassirugata* del Río & Camacho, *Neilo ornata* (Sowerby), *Arca patagonica* Ihering, *Crassostrea hatcheri* (Ortmann), and the echinoid *Iheringiella patagonica* (Desor).

DS 2: The lens yielding samples of *Retrotapes striatolamellatus* is ca. 16 masl and was dated at 18.81 Ma (Parras et al., 2012). Associated fossils are *Turritella ambulacrum,* disarticulated *Cucullaea alta,* articulated *Limopsis insolita* Sowerby and brachiopods.

DS1 and DS2 are both from the lower part of the MLF deposited in a transitional environment between the inner shelf and a subtidal plain, below fair-weather wave base and above storm wave base (Parras and Griffin, 2009).

DS 3: This sample (*Retrotapes striatolamellatus*) comes from lenses of fine tuffaceous sandstone in the middle part of the section, ca 50 masl. There is no age control for this bed, but an estimated age assuming the average sedimentation rate of ca 50 m/Myr calculated by Parras and Cuitiño (2018) places this horizon ca 18.15 Ma.

This lens is poorly fossiliferous and contains *R. striatolamellatus*, broken *Cucullaea alta*, and scarce *Dosinia meridionalis* Ihering, but laterally it becomes one of the most highly diverse fossiliferous horizons of the MLF from which all the described fauna of the unit come. This middle part of the MLF is inferred to represent a subtidal environment at the lowest part of a tidal flat, in shallower waters than DS1 and DS2 (Parras et al., 2012).

Cañadón Los Misioneros section (49° 59′ 19.28″S; 68° 33′ 20.03″W) is situated 3.4 km north of Puerto Santa Cruz and 19 km north of the Darwin section. The sedimentary sequence consists of a lower 40 m section of tuffaceous mudstones containing thick (≤30 cm) intercalated fossiliferous lenses, followed by 20 m of tuffaceous sandstones capped by two massive, yellowish fossiliferous beds. Our sample CLM (*Cucullaea alta*) comes from the uppermost bed and is associated with a diverse molluscan fauna containing *Darwinicardia patagonica* Sowerby, *Panopea quemadensis* Ihering*, Ameghinomya meridionalis* Sowerby*, Lahillia patagonica* Ihering, *Neilo ornata* (Sowerby), *Limopsis insolita* (Sowerby), *Neopanis quadrisulcata* (Ihering), *Retrotapes striatolamellatus* (Ihering), *Miomelon gracilor* (Ihering), *M. dorbignyana* (Philippi), *Adelomelon pilsbry* (Ihering), *Perissodonta ameghinoi* (Ihering), *Polinices santacruzensis* Ihering, and *Glossaulax secundum* (Rochebrune and Mabille), among others. Age control is not available for this horizon, but we can place it with confidence as being stratigraphically above the Darwin section samples and below the Las Cuevas sample, and hence we use an estimated age of 18 Ma for the purpose of plotting data.

Las Cuevas–Monte Observación section: The base of this section was measured 47 km south of the mouth of the Santa Cruz River, at Las Cuevas [50° 22′ 54.82″S; 68° 55′ 31.94″W] and the upper part was measured at Monte Observación [50° 21′ 50.52″S; 68° 58′ 40.06″W]. Studied material derives from two horizons:

LC: This sample (*Austrocallista iheringii*) comes from a 3.5 m thick, yellowish, cross-bedded, bioclastic, fine to medium-grained sandstone with disseminated shell placed at 28 masl and dated at 17.91 Ma (Parras et al., 2012). This bed can be easily recognized along the coast for almost 20 km and constitutes the first topographic step in the sea cliffs. It belongs in "Facies Association 1" of Parras and Cuitiño (2018), deposited in inner-shelf to lower-shoreface environments (A. Parras, *pers. comm.*). It is characterized by the highest fossil concentration of the entire sequence exposed in the area, and its fauna is highly diverse, inhabiting environments with normal salinity

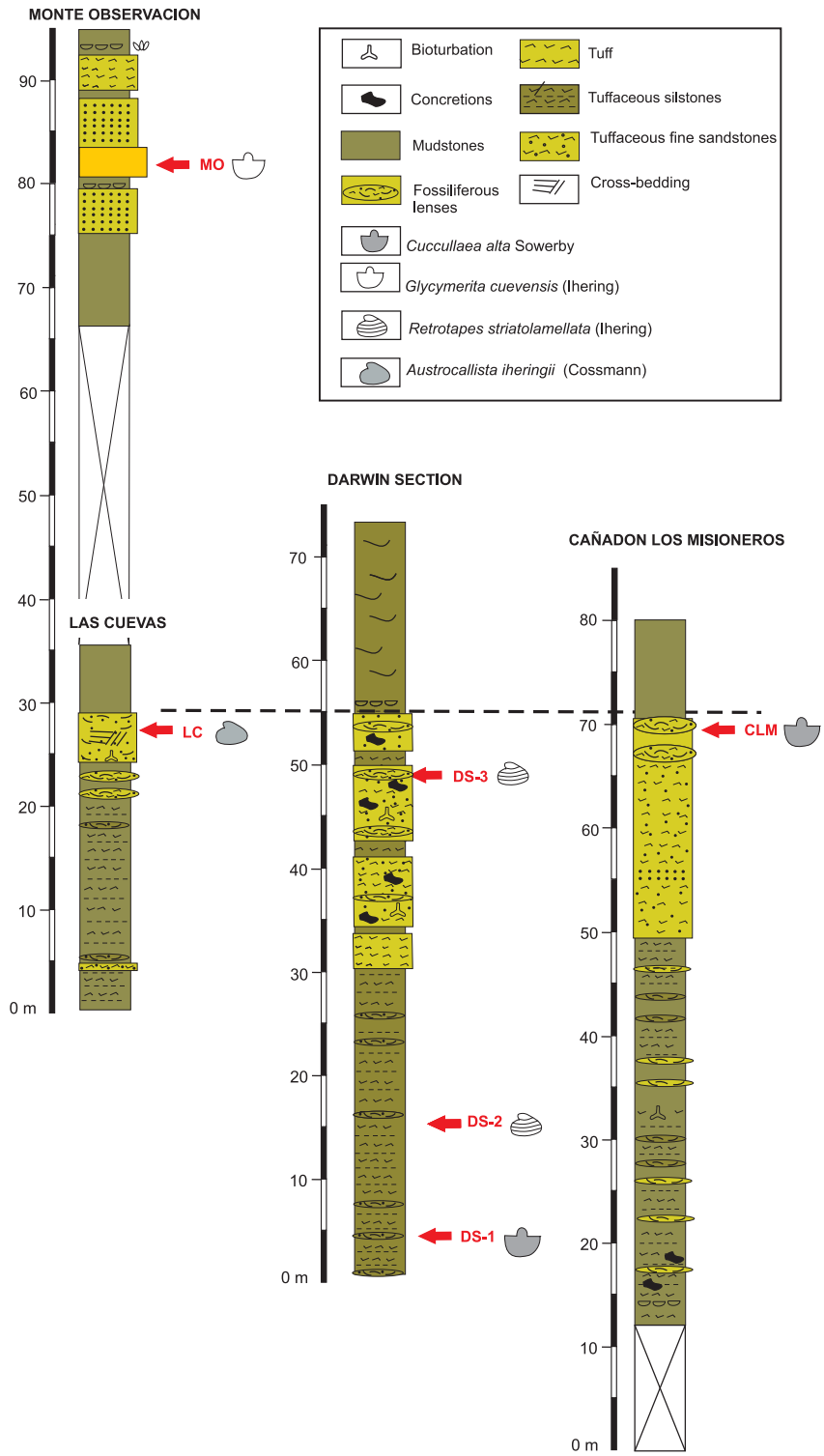

Figure 4. Stratigraphic sections of the Monte León Formation studied here, indicating sampled horizons and inferred correlations. Abbreviations as in Figure 1b.

and mainly represented by abundant, well-preserved shells of "*Turritella*" sp., *Reticulochlamys proximus* (Ihering), *Neoimbricaria quemadensis* (Ihering), *Cirsotrema rugulosa* (Sowerby), *Darwinicardia patagonica* (Sowerby), *Osterheldia cannada* (Ihering), *Dosinia meridionalis* Sowerby, *Austrocallista iheringii* (Cossmann), *Adelomelon cannada* (Ihering) and *Miomelon gracilor* (Ihering), among others.

MO: This fossiliferous bed is positioned at ca 82 masl (*Glycymerita cuevensis*) in the Monte Observación Member and is represented by a 0.5 m thick, massive, brown-green, medium to coarse-grained sandstone. The fauna is low diversity, and is represented by abundant, well-preserved, entire and disarticulated valves of *Glycymerita cuevensis* and *Crassostrea hatcheri* (Ortmann) and by large and entire shells of *Pachycymbiola ameghinoi* Ihering, along with fragmented and sometimes eroded valves of *Ameghinomya* sp., *Austrocallista iheringii*, *Retrotapes striatolamellata* (Ihering) and *Molvaldesia* sp. Shells are loosely disseminated throughout rather than packed into a shell bed.

No direct age control is available, but the average sedimentation rate of 230 m/Myr calculated by Parras and Cuitiño (2018) places this horizon at ca 17.69 Ma, slightly younger than had been suggested for the top of the formation by Perkins et al. (2012). This bed, as well as the horizons with *Crassostrea hatcheri* in life-position situated below and above, is interpreted as accumulating during flooding in interdistributary bays of a delta, where opportunistic marine species colonized the substratum during intervening times of normal salinity (Parras and Cuitiño, 2018).

3.3. Stable Oxygen Isotope Sampling and Analysis

Shells chosen for stable isotope analysis are complete, well-preserved, and bear little to no evidence of wear or bioerosion. Freshly broken shell fragments were examined under scanning electron microscopy (SEM) using the JEOL NeoScope JCM-6000 Plus at Syracuse University to evaluate preservation of shell microtextures. Twenty shells were sampled for stable oxygen ($\delta^{18}O_{carb}$) and carbon ($\delta^{13}C_{carb}$) isotope analysis. Three time-integrated samples of shell carbonate were collected from the cleaned exterior surface of each valve using a VMax dental drill: one near the umbo, one in the middle of the valve, and one near the ventral margin, so as to constrain average shell composition. Additionally, four of these shells (one of each taxon, spanning the stratigraphic section) were chosen for serial sampling at high spatial/temporal resolution across portions of the ontogeny using a Merchantek/New Wave/ESI MicroMill in the Paleoecology Laboratory at Syracuse University in order to constrain intra-annual temperature variation. Sampling was conducted on the cleaned exterior shell surface using a series of closely spaced, growth-band-parallel, milling lines. Sampling begins as close to the umbo as possible (as soon as shell curvature allows digitization and sampling of three-dimensional milling paths on a flat-lying shell beneath a vertically oriented drill) and proceeds through ontogeny across several prominent (presumed to be annual) growth increments. Samples were analyzed for their stable oxygen and carbon isotopic compositions using a Finnegan MAT 251 or 253 mass spectrometer coupled to a Kiel automated carbonate preparation device at the University of Michigan Stable Isotope Laboratory. Data are reported relative to the Vienna PeeDee Belemnite (VPDB) standard and were corrected using international reference materials NBS-18, NBS-19, and Carrera. Average precision is better than 0.04‰.

3.4. Seasonally Resolved Data

Sequential, subannually resolved, oxygen isotope data for each shell are fit with best-fit sinusoids (Judd et al., 2018) to minimize the influence of noise in the isotope data that define the annual cycle and to correct for intra-annual changes in shell growth rate that can bias average shell $\delta^{18}O$ values (Goodwin et al., 2003). This approach yields more accurate estimates of MAT and seasonal extremes from accretionary biogenic carbonates (Ivany and Judd, 2022; Wilkinson and Ivany, 2002). For each shell, we fit sinusoids through successive subsets of the data, determine the mean, winter, and summer values for each subset, and then use their means and standard deviations to determine the overall best-fit annual cycle described by the data from each shell. We use the parameters of the best-fit sinusoids to compare to climate model output.

3.5. Paleotemperature Calculations

Paleotemperatures are calculated from $\delta^{18}O_{carb}$ values using the empirically derived biogenic aragonite paleotemperature equation of Grossman and Ku (1986) as updated by Hudson and Anderson (1989). The $\delta^{18}O$ value of seawater requisite in the calculation can be difficult to constrain (see Section 5.1). Here, we derive $\delta^{18}O_{sw}$ from

the global average seawater composition at 18 million years estimated by Lear et al. (2015) based on the $\delta^{18}O$ values of benthic foraminifera in combination with temperatures determined from their Mg/Ca ratios (Lear et al., 2000). We used the calibrations of Lear et al. (2002, 2010) to yield two estimates of global average composition (−0.3 and −0.6‰, respectively, for a mean of −0.45‰), with the difference between them reflecting the uncertainties associated with calculating temperatures from foraminiferal Mg/Ca ratios (Lear et al., 2015). Acknowledging that sea-surface $\delta^{18}O$ values vary over Earth's surface today (LeGrande and Schmidt, 2006), the global seawater value is then adjusted for a paleolatitude of 54°S (van Hinsbergen et al., 2015) using the relationship in Zachos et al. (1994) describing the variation in modern sea surface compositions with latitude, here a change of only −0.04‰. This adjustment assumes that the latitudinal gradient of sea-surface $\delta^{18}O$ values from today can be reasonably applied to the Miocene ocean, likely an oversimplification, but it nevertheless accommodates some degree of the expected spatial heterogeneity. The two values were then averaged to yield a best estimate of local Miocene seawater of −0.49‰.

3.6. Comparison With a Coupled Climate Model

We interpret our proxy data in the context of previously published fully coupled Miocene paleoclimate simulations (Acosta et al., 2022; Gaskell et al., 2022) using the water-isotope-enabled Community Earth System Model version 1.2 (iCESM1.2) (Brady et al., 2019). The model estimates mean monthly SST in the vicinity of our samples and allows for spatial variability in the $\delta^{18}O$ value of surface seawater (LeGrande and Schmidt, 2006) and the effect of seawater carbonate concentration (pH) on sea-surface carbonate $\delta^{18}O$ value (Zeebe, 2001). Our implementation of iCESM uses the Community Atmospheric Model version 5 (CAM5) with water isotope physics. The iCAM5 interacts with the isotope enabled version of the Community Land Model version 4, the Sea Ice model, Parallel Ocean Program version 2 and a river transport. The simulations were carried out with CO_2 levels of 400 and 560 ppm, under finite volume dynamical core version of the atmosphere model and have a grid spacing of 1.9° × 2.5°, equal to ∼200 km over the equator. Ocean and sea-ice models have a nominal 1° resolution. The orbital forcing, solar forcing, and greenhouse gases other than CO_2 were set at Preindustrial levels. We use the updated Middle Miocene (∼17–14 Ma) boundary conditions (Burls et al., 2021), which simulates an open Drake Passage, and use plate rotations from Matthews et al. (2016). The isotopic composition of seawater ($\delta^{18}Osw$) was initialized from values in the Preindustrial simulation and allowed to equilibrate. Note that plate rotations from Matthews et al. (2016) yield a slightly lower paleolatitude than the estimate using van Hinsbergen et al. (2015); but the resulting local seawater offset only changes by 0.1 per mil and equates to only about a half a degree of difference in calculated paleotemperatures. Simulations were continuously run for over 2,000+ years to allow the models to reach steady state in both the atmosphere and deep ocean. Simulations have minimal top of the atmosphere (TOA) energy imbalances of 0.17, and 0.15 W m^{-2}, respectively, with global mean surface temperature of ∼19 and ∼21°C. The last 100 years of the simulations were used to calculate the climatology files. Output from the simulations have been previously used to study hydroclimate evolution in South America across the Cenozoic (Acosta et al., 2022) and Europe and North Africa during the MCO (Acosta, Burls, Pound, Bradshaw, McCoy, et al., 2024), and have been used in DeepMIP Miocene to understand changes in the global hydrological cycle (Acosta, Burls, Pound, Bradshaw, De Boer, et al., 2024). We divide samples into Early Miocene (∼19 Ma) and Early Middle Miocene (∼17.75 Ma) and compare calculated proxy temperatures with simulations run at 400 and 560 ppm CO_2, respectively. We omit direct comparison of proxy $\delta^{18}O_{carb}$ to modeled $\delta^{18}O_{carb}$ using modeled $\delta^{18}O_{sw}$ and temperature because potential mismatch could be due to multiple unresolved factors (see Section 5.1). Hence, we primarily focus on comparisons of SST estimates.

4. Results

Polished shell cross sections reveal growth bands associated with changes in the proportion of organic shell matrix and/or the degree of order of carbonate crystals that reflect changes in the rate of shell accretion with time (Figure 5). In extra-tropical shells, primary bands are generally annual in nature and associated with seasonal environmental variation, an hypothesis that can be verified with high-resolution accretionary stable isotope data (Jones and Quitmyer, 1996).

SEM imagery of shell fragments reveals that original microtextures are preserved (Figure 6). *Austrocallista*, *Glycymerita*, and *Cucullaea* display crossed-lamellar textures, and *Retrotapes* exhibits poorly organized homogeneous and crossed acicular textures similar to *Arctica islandica* today (see Dunca et al., 2009). Minor dissolution is evident in some shells (e.g., Figure 6b), but no secondary precipitates were observed. Preservation

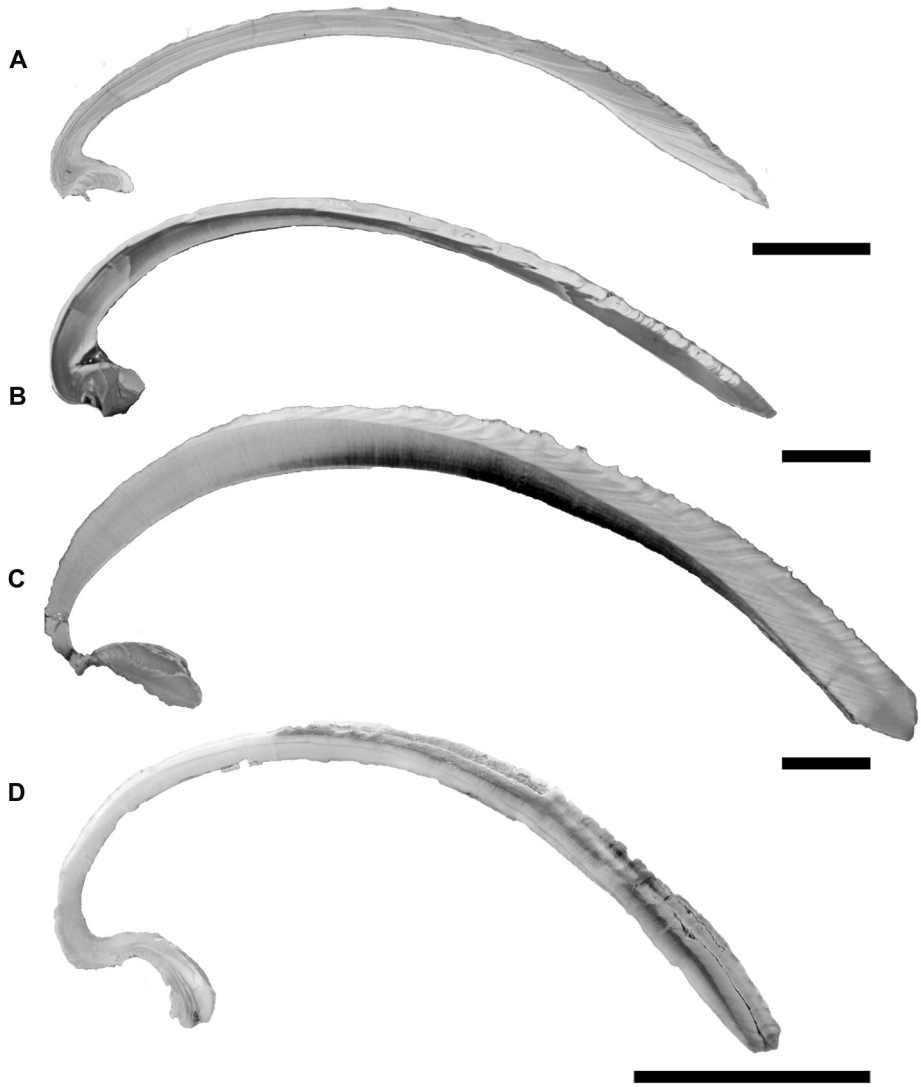

Figure 5. Cross section of the studied shells. (a), *Retrotapes striatolamellatus*, CPBA 9359B, Darwin Section (DS2). (b), *Austrocallista iheringi*, CPBA 9389B, Las Cuevas (LC). (c), *Glycymerita cuevensis*, CPBA 16622, Monte Observación (MO). (d), *Cucullaea alta*, CPBA 16605, Darwin Section (DS1). Scale bar = 10 mm.

index as per Cochran et al. (2010) and Knoll et al. (2016) generally hovers between 4 and 5, with the somewhat leached crossed-lamellar fabrics of *Austrocallista* scoring 3.5.

Oxygen isotope values of individual bulk shell carbonate samples from the MLF range from −1.21 to 1.06‰. Horizon-mean values decrease upsection from around 0.5 to −0.65‰, with most of the change occurring between 18.15 and 17.69 Ma (Figure 7). Calculated paleotemperatures using the Mg/Ca-calibrated and latitude-adjusted local seawater $\delta^{18}O$ value of −0.49 increase upsection from a mean around 15°C at 19.27 Ma to around 20°C at 17.69 Ma, just prior to the onset of the MCO (Figure 7).

Seasonally resolved accretionary data (Figure 8) are consistent with the range of bulk shell samples and provide insights into the rate and timing of growth for each taxon. Plots of $\delta^{18}O$ versus distance along the growth axis for each taxon reveals that *Cucullaea* precipitates more shell in the winter-spring months, *Glycymerita* and *Austrocallista* preferentially grow in the summer, and *Retrotapes* more in the spring and summer. While the amount of shell growth differs with season, all four taxa capture seasonal extremes well early in their ontogenies. *Glycymerita* is evidently a slow-growing, long-lived taxon based on its large size and the number of years captured by the isotope data (Figure 9), consistent with the closely spaced growth banding visible in Figure 5c. This taxon in

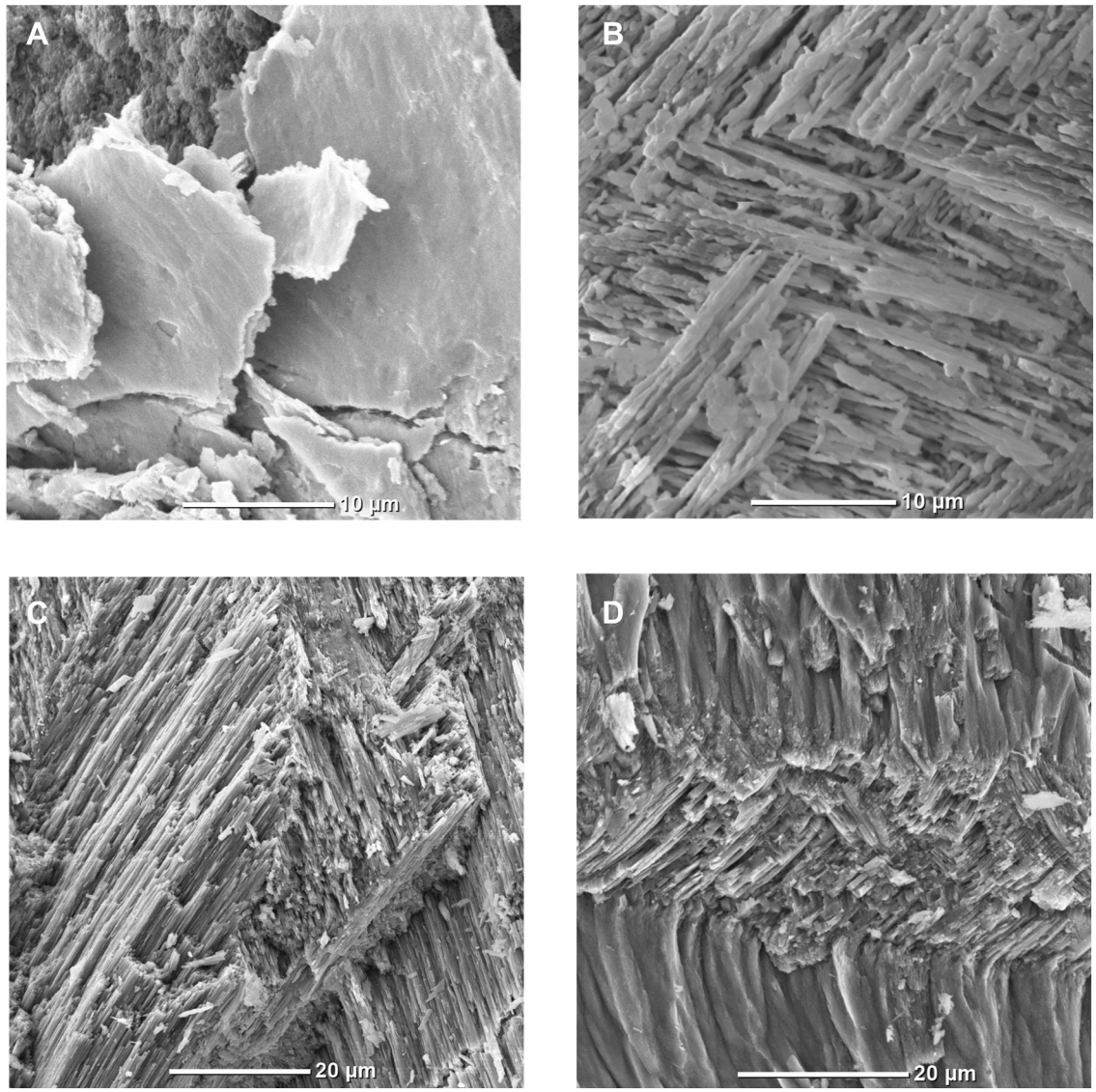

Figure 6. Scanning electron microscopy images of shell microtextures. (a), Poorly organized homogeneous textures in *Retrotapes striatolamellatus*, CPBA 9359C, Darwin Section (DS2), PI = 5. Crossed lamellar textures in panel (b), *Austrocallista iheringi*, CPBA 9398C, Las Cuevas (LC), PI = 3.5, showing minor dissolution; (c), *Glycymerita cuevensis*, CPBA 16619, Monte Observación (MO), PI = 5; and (d), *Cucullaea alta*, CPBA 16605, Darwin Section (DS1), PI = 4. PI (preservation index sensu Cochran et al., 2010).

particular could therefore underestimate the magnitude of seasonal extremes due to the greater degree of time-averaging of individual accretionary samples as one moves farther from the umbo, and average shell values are more likely to be shifted toward the preferred (summer) season of growth later in ontogeny.

Parameters defining the best-fit sinusoids for each year of growth confirm the seasonal timing of growth and yield growth-corrected estimates of the annual temperature cycle for their respective stratigraphic positions (Figure 10). With respect to growth, the arithmetic means of shell samples from *Glycymerita* and *Austrocallista* are −0.70‰ and −0.06‰, respectively, while the best-fit sinusoid means are −0.64‰ and +0.06, respectively. As well, in the well-sampled LC horizon, "bulk" (average) shell data are slightly offset from the best-fit estimate of MAT derived from *Austrocallista*. Each of these offsets is in a direction consistent with preferential shell growth in the summer, illustrating how raw sample data can give a somewhat biased mean temperature if the preferred season of shell growth is not taken into consideration. In general though, seasonally constrained data from individual shells overlap the range defined by bulk samples well and augment the information on mean composition and temperature that they provide. Seasonal temperature range defined by best-fit shell data increases upsection from

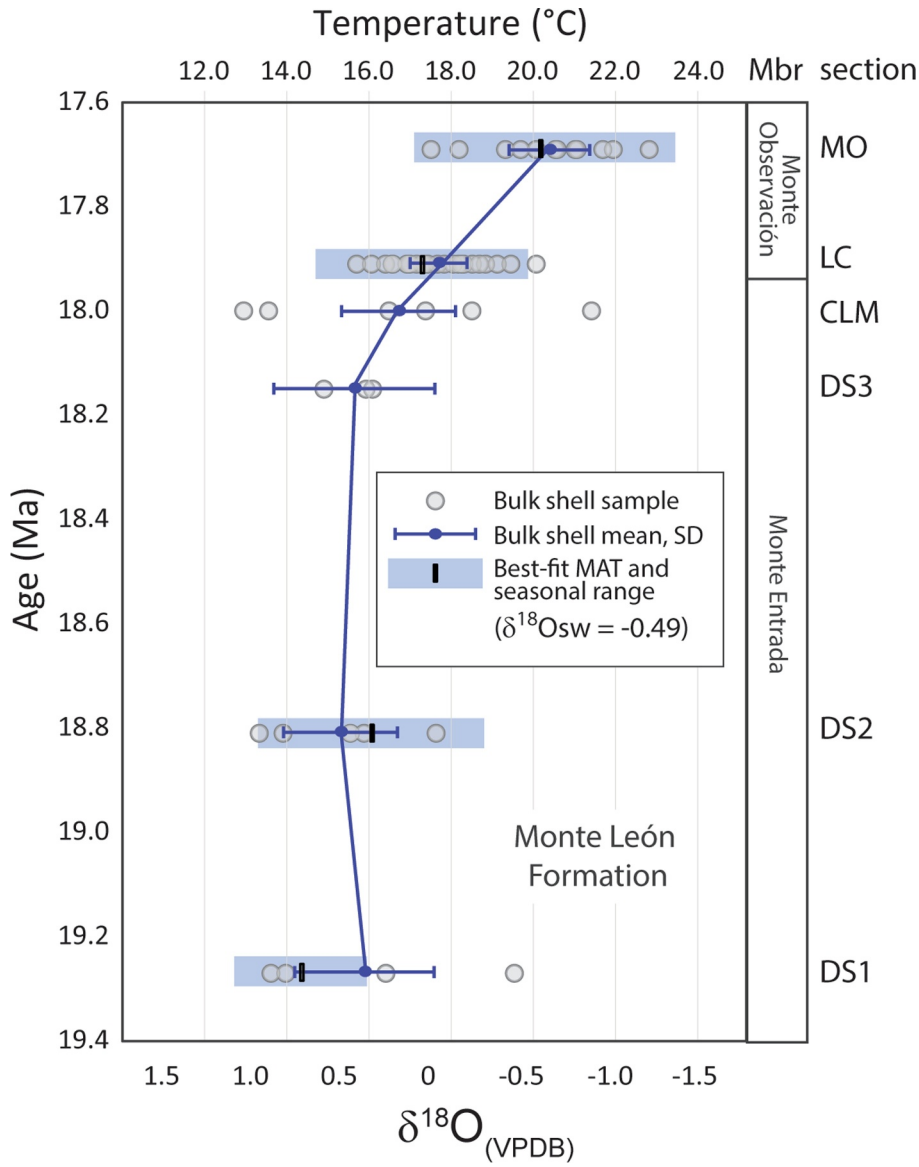

Figure 7. Paleotemperatures through the Monte León Formation (Burdigalian) calculated using δ^{18}Osw = −0.49‰. Reported are bulk shell isotope values, their horizon means, and the mean and seasonal range derived from seasonal data in Figure 8. Age control is based on field-based stratigraphic relations and geochronology from Parras et al. (2012).

3.5°C to 6.3°C (Figure 10), accomplished through warming of summer temperatures (+7.6°C) more than winters (+4.7°C).

Paleoclimate simulation of 400 ppm CO_2 shows mean annual SST ranging from 13.7 to 15.4°C off the Patagonian coast, comparable to proxy data from our older samples; the 560 ppm CO_2 simulation shows SSTs ranging from 15.6 to 17.3°C, more in line with our younger samples (Figure 11). Paleoclimate simulations of austral winter (JJA) SST range from 11.5 to 13.2°C at 400 ppm and 13.1–14.8°C at 560 ppm, while austral summer (DJF) SST ranges from 16.6 to 18.1°C and 19.0–20.3°C, respectively (Figures 12 and 13). Again, older proxy data are more in line with the 400 ppm simulation while younger fit the 560 simulation better. Our uppermost (youngest) sample yields proxy data 3–4°C warmer than the model in both winter and summer (Figure 13). Model seasonal range increases from about 5 to 5.7°C with increasing pCO_2.

All stable isotope data and summary curve-fit statistics are available from the Zenodo repository using the link in the Data Accessibility Statement at the end of this paper.

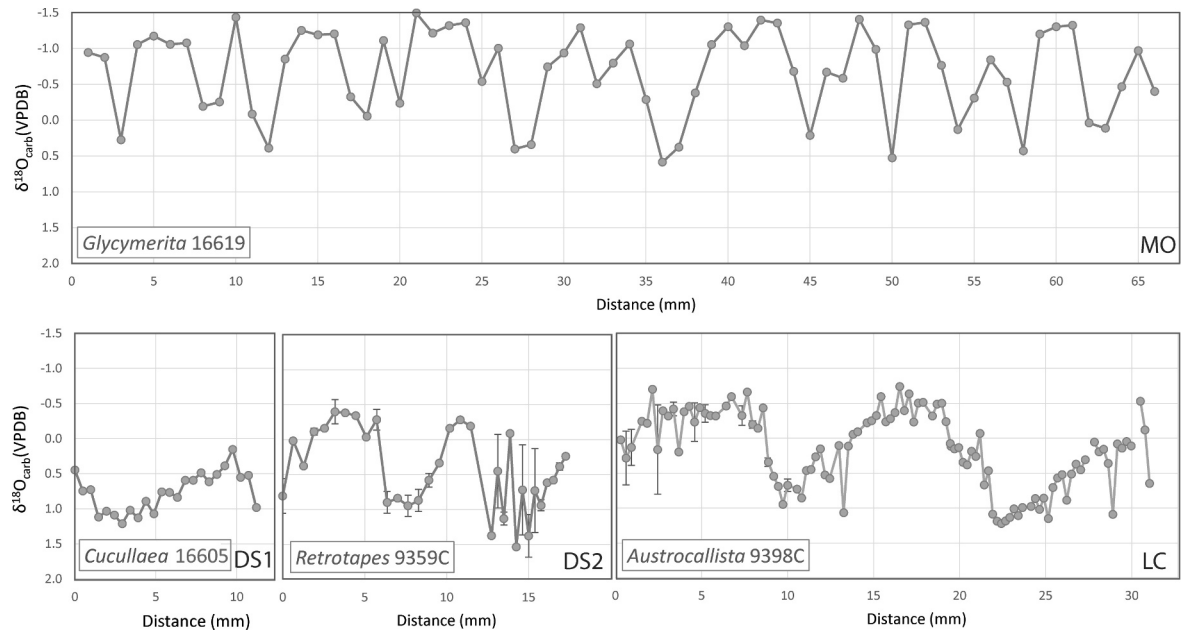

Figure 8. Seasonally resolved $\delta^{18}O$ data for each taxon derived from micromilling. Only a portion of shell ontogeny is covered by the data (see Figure 9 for locations of data along growth axis). Stratigraphic horizon is indicated in lower right—see Figure 7 for position. Axes are scaled the same for each plot.

5. Discussion

5.1. Uncertainty Surrounding the Isotope Value of Seawater

The main source of uncertainty in calculating paleotemperatures from carbonate $\delta^{18}O$ values is in the $\delta^{18}O$ value of the seawater from which the carbonate precipitates, a variable for which there are no direct and uncomplicated proxies. Lear et al. (2000) pioneered the use of a second independent proxy system to estimate paleotemperatures and then calculate water composition given measured carbonate $\delta^{18}O$ values, applying this approach to the record of Mg/Ca and $\delta^{18}O$ of benthic foraminifera in order to back out the $\delta^{18}O$ value of global mean seawater over the Cenozoic. Nevertheless, uncertainties related to the calibration of foraminiferal Mg/Ca to temperature, the changing Mg/Ca ratio of seawater over the Cenozoic, and the potential influence of pH, salinity, and saturation state can introduce error (Lear et al., 2015; Lowenstein and Hönisch, 2012; Modestou et al., 2020).

There are reasons to suspect that our estimate of $\delta^{18}O_{sw}$ is a reasonable one. Gasson et al. (2016) use an isotope-enabled GCM to model ice sheet growth starting from ice-free conditions under their "warm climate" simulation with mid-Miocene bedrock topography (their Scenario B) and produce an Antarctic ice sheet with the equivalent of a +0.48 per mil increase in global seawater $\delta^{18}O$. This yields a global seawater value, starting from an ice-free ocean at −1.0‰, of −0.52‰, close to our estimated global mean value of −0.45‰ using Lear et al. (2015). Likewise, our estimated sea-surface offset from global mean seawater based upon paleolatitude is small (−0.04‰). Because the Miocene CESM1.2 climate model is isotope-enabled, local/regional offsets from the global mean seawater $\delta^{18}O$ value are apparent in the spatial variation of modeled surface seawater $\delta^{18}O$ and can be compared to the independently generated offset derived from the relationship in Zachos et al. (1994). The model indicates a local offset from the global mean of between 0 and −0.1‰ (not shown), in good agreement and suggesting that heterogeneity in sea-surface $\delta^{18}O$ is reasonably captured as well.

Other published estimates of $\delta^{18}O_{sw}$ bracket our global value. A detailed synthesis of benthic paleotemperature records and sea-level estimates for the purpose of estimating changes in ice volume over much of the Cenozoic yielded estimates of deep-sea $\delta^{18}O$ (Rohling et al., 2022). During the Burdigalian, their envelope of uncertainty spans between about −0.50 and −0.75‰, in the range of or somewhat lower than ours and equating to temperature uncertainty of around 1°C toward cooler temperatures, with no long-term trend between 17 and 19 Ma. An extreme alternative in the opposite direction is presented by clumped isotope-derived estimates of deep-sea $\delta^{18}Osw$. A careful study of paired clumped isotope and Mg/Ca paleotemperatures off NE Australia shows good agreement between the two proxies, yielding very warm benthic temperatures during the MCO (Modestou

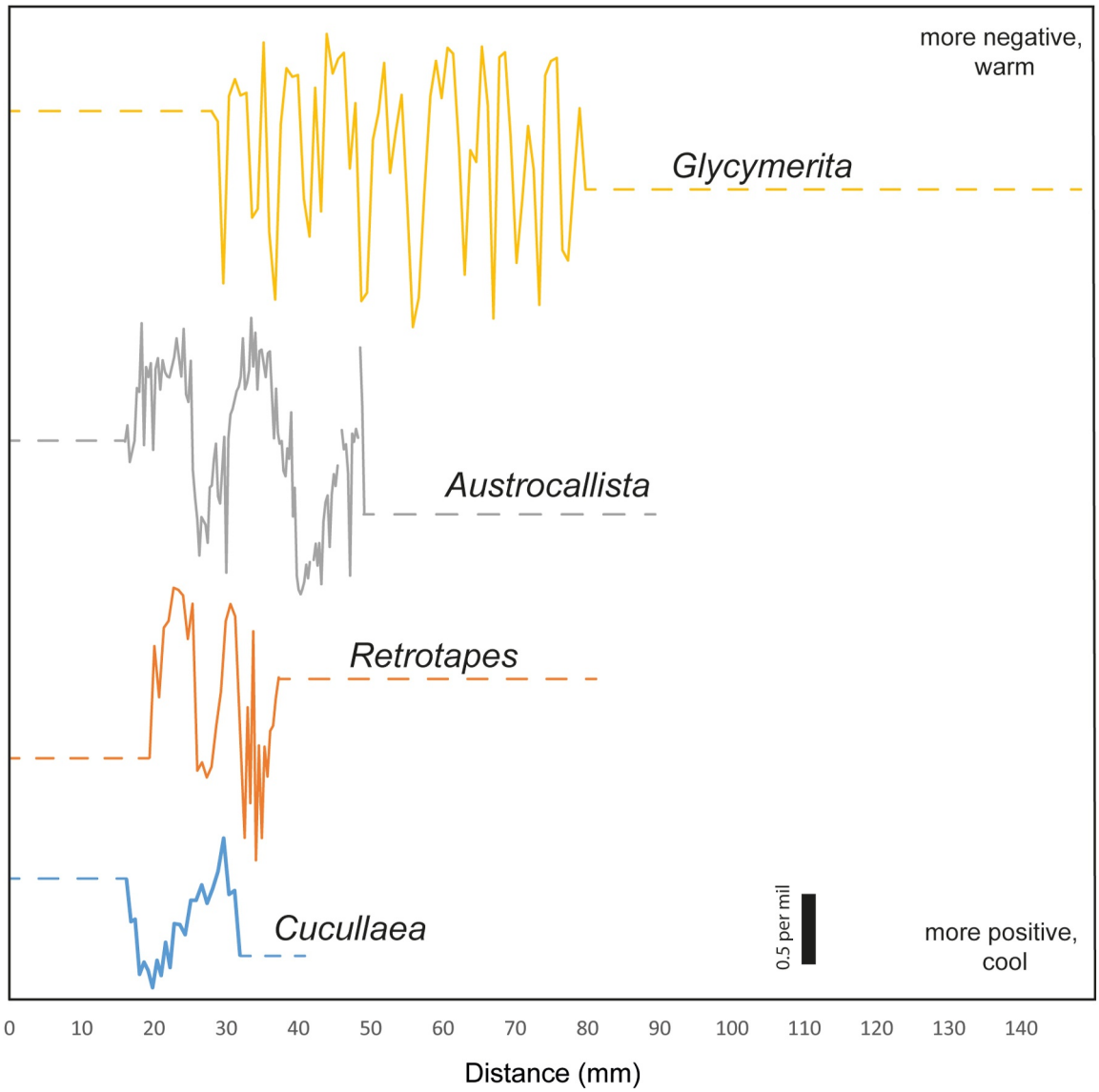

Figure 9. Comparison of growth rates for each taxon over their respective ontogenies. Size of individuals sampled for each taxon is represented by a dashed line from umbo to commissure, with solid portion indicating the position on the shell from which the isotope data come. Variation in the *Y* axis for each reflects years of growth in that portion of ontogeny as revealed by stable isotope data and is scaled the same for each plot (with more negative, warmer, toward the top in each).

et al., 2020), and these are reinforced by similarly warm clumped isotope paleotemperatures for deep water in the southern Indian (Leutert et al., 2021) and the north Atlantic Oceans (Meckler et al., 2022) over longer intervals of time. In combination with $\delta^{18}O_{carb}$ values from Westerhold et al. (2020), these data call for global seawater values around +0.5‰—and an ice sheet larger than today's or alternative explanations for shifting global $\delta^{18}O_{sw}$ (e.g., Meckler et al., 2022)—before and during the MCO. This is an unexpected and surprising result, with significant implications for Earth system sensitivity (e.g., Ring et al., 2022), but it is perhaps too soon to know whether this value will be supported by additional work (though see Evans, 2021). Treating this value as an endmember possibility yields calculated early Miocene Patagonian temperatures that are warmer by about 4°C, putting them well above estimates derived from the coupled climate model (Figure 11) and as much as 12°C warmer than the few TEX_{86}-derived temperatures from the MCO in the Scotia Sea (Hoem et al., 2023). Uncertainty in the global composition of seawater therefore results in an envelope of mean temperatures that range from 1°C cooler to perhaps as much as 4°C warmer than those we report here.

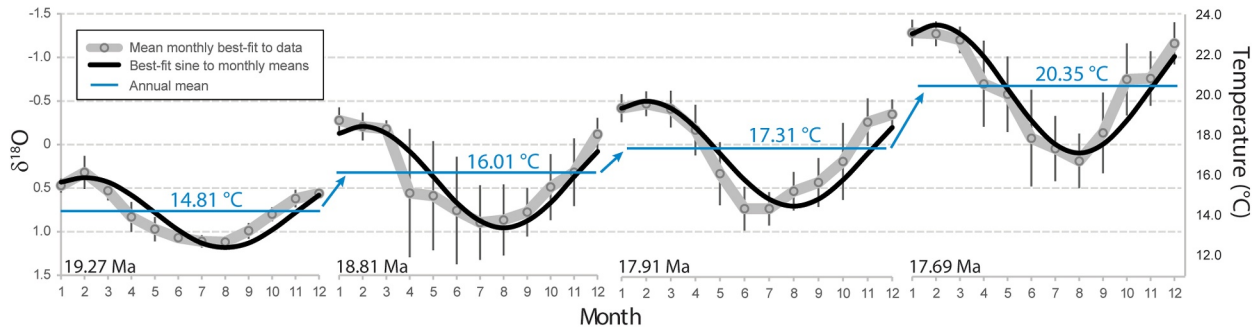

Figure 10. Change in the annual temperature cycle through time in the Monte León Formation. Monthly means and standard deviations are determined from best-fit sinusoids through successive subsets of the data in Figure 8 (see Section 3.4). Annual cycles are constrained by, left to right, 5, 17, 39, and 39 sine-fit subsets of data. Best overall sinusoid (black) is fit to the monthly mean values derived from curve fits, with February (month 2) set as the warmest month. Mean annual temperature for each time interval is given in blue using δ^{18}Osw = −0.49. Summer temperatures at 19.27 Ma could be underestimated due to summer growth cessation.

A $\delta^{18}O_{sw}$ value of ∼−0.5‰ suggests an Early Miocene global ice volume approximately half that of today, an intuitively satisfying estimate for a time of generally warmer climate with an Antarctic ice sheet of some proportion. Our assumption of a single consistent seawater value over ∼2 million years of the Early Miocene, however, is an oversimplification. Sediment cores in McMurdo Sound and the Ross Sea, Antarctica, suggest a highly variable Early Miocene ice sheet in that area, ranging from ice-free temperate shorelines to a grounding line beyond what it is today (Levy et al., 2016; McKay et al., 2024; Passchier et al., 2011), with presumably concomitant variation in $\delta^{18}O_{sw}$ that we would interpret as temperature. Coupled ice-sheet and climate models support large-scale ice advances and retreats in the early-mid Miocene (Halberstadt et al., 2021). While short-term fluctuation in the benthic foraminiferal $\delta^{18}O$ and Mg/Ca records is present and might be attributed to high-frequency climate variation, including changes in ice volume (and $\delta^{18}O_{sw}$), we are hesitant to overinterpret shifts constrained by only one or a few data points and opt instead to choose a single representative seawater $\delta^{18}O$ value based on Lear et al. (2015) for the temporal window spanning our samples. The Rohling et al. (2022) synthetic record suggests high-frequency $\delta^{18}O_{sw}$ variation on the scale of <0.2‰, equating to potential temperature swings of a degree or less that might be subsumed within our record - not enough to change the overall pattern through time. Immediately before our oldest samples, however, between ∼20 and 19.5 Ma, two distinct pulses toward more positive values in both $\delta^{18}O_{carb}$ (∼1‰) and $\delta^{18}O_{sw}$ (∼0.3‰) likely reflect ice growth and cooling that, with only minor adjustments to our age model, might have influenced our samples. Interestingly (though perhaps purely coincidentally), these roughly correspond to the timing of a marked extinction in pelagic sharks documented by Sibert and Rubin (2021) that immediately precedes our data.

In sum then, acknowledging the uncertainty discussed above, the available data suggest that global $\delta^{18}O_{sw}$ (a) exhibited no long-term trend over the window encompassed by our samples, (b) varied by <0.2‰ within that interval, and (c) most likely hovered near our estimated value of −0.45‰. We therefore discuss our stable isotope results in this framework, using a latitude-adjusted local value of −0.49‰. With increasing clarity on this global value and its range of variation in both space and time, interpretations drawn from our stable isotope data can be adjusted.

5.2. Monte León Formation Paleoclimate Record

Bivalve associations in the MLF imply normal or near-normal marine salinities. Shell mineralogy, microtextures, and taphonomy suggest generally excellent preservation of in situ shell material. Values of, and trends and variation in, stable oxygen isotope data can therefore be reasonably interpreted to reflect original paleoenvironmental conditions in high-latitude Patagonia during the Early Miocene.

If our estimate of regional seawater $\delta^{18}O$ is correct, and if seawater values were consistent over the time spanned by our data, as we argue, then mean proxy temperatures hover between 15 and 16°C until ca. 18 Myr, at which point temperatures begin to warm, reaching ∼20°C by 17.69 Ma (Figure 7). A warming trend is consistent with the transition into the MCO. Seasonal range increases upsection as well, and suggest warming in the summer more than in the winter (Figures 8 and 10). Temperatures in the lowermost horizon are constrained by comparatively few data, and seasonal range by only 1 year of data from a taxon that grows preferentially in the winter. While

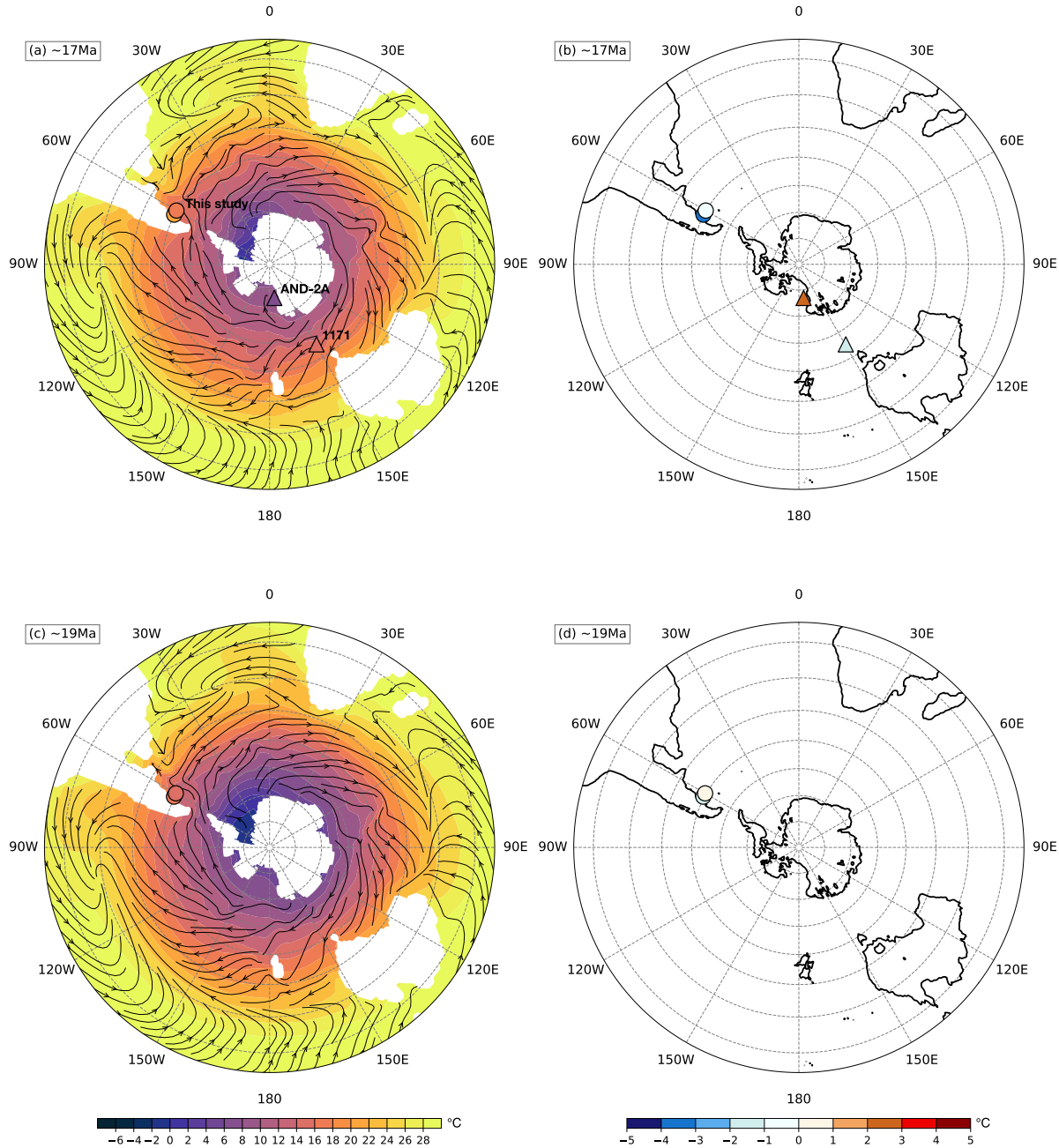

Figure 11. Proxy-Model comparison (a) and (c) and anomaly (b) and (d) of mean annual sea surface paleotemperatures derived from iCESM1.2 Miocene paleoclimate simulation. Simulations show 560 ppm (a) and (b) and 400 ppm (c) and (d). Plotted data are the best-fit MATs from shells in the upper two horizons (a) and (b) and lower two horizons (c) and (d) from this study (circles), along with compiled sea-surface temperature proxy data (triangles) from Burls et al. (2021).

summer temperatures and hence seasonally resolved MAT here might be underestimated, the span of the bulk shell data generally overlaps that of the horizon above. In the absence of additional data, we therefore consider both horizons to indicate ~ similar conditions and hence that the better-constrained seasonally resolved data from 18.8 Ma indicate an increase in seasonal range upsection from ~5 to 6.3°C.

The question of whether the more negative isotope data from the uppermost, youngest, Monte Observación (MO) horizon reflect a true indication of warming or a decrease in water composition associated with a drop in salinity is worthy of further investigation. The micromilled data from *Glycymerita* can provide insight. Growth banding and isotope data both suggest a long-lived animal, recording many years of growth over its lifespan. That the isotope data from successive winters and summers are reasonably consistent from year to year at least over the ~10 years

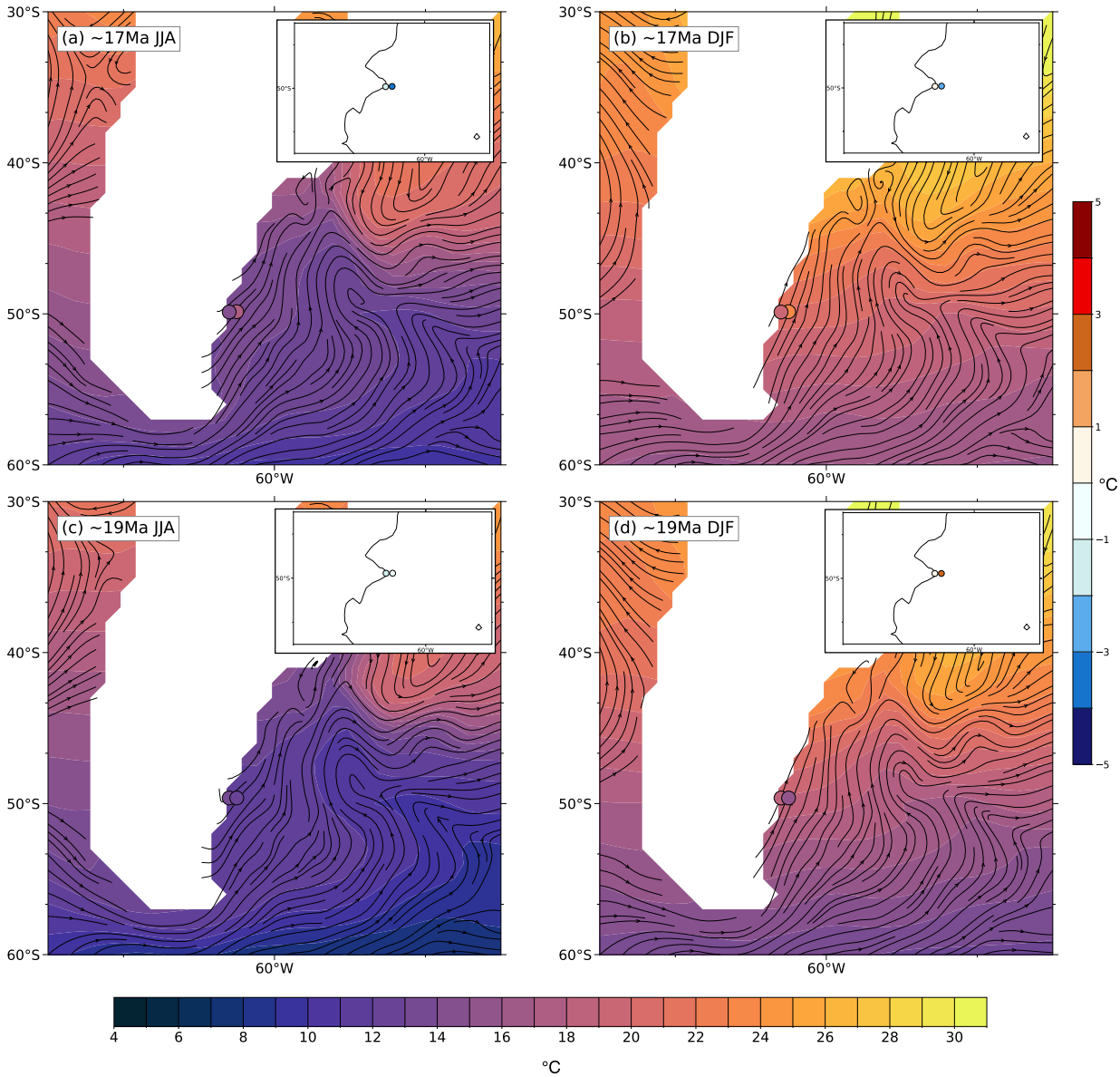

Figure 12. Proxy-model comparison of austral winter (a) and (c) and austral summer (b) and (d) sea surface paleotemperatures derived from iCESM1.2 Miocene paleoclimate simulation. Simulations show 560 ppm (a) and (b) and 400 ppm (c) and (d) scenarios. Plotted data as in Figure 11, from best-fit seasonal extremes. Inset shows data-model anomaly of mean annual sea surface paleotemperatures.

sampled, and that the taxon is evidently quite long-lived given its large size, the relatively small and early portion of its ontogeny represented by those data, and the expectation that annual shell growth only slows with age (Figure 9), both point to a stable predictable environment, unlike what one would expect in a setting with reduced salinity. Brackish environments are instead likely to be intra- and interannually variable in salinity and $\delta^{18}O$, as water isotope values from such places are strongly controlled by salinity and the vagaries of storm tracks, including the region from which moisture evaporated, the amount of precipitation, the elevation and temperature at which it falls, and the degree of evaporation en route. Therefore, the shift to warmer and more seasonal proxy-derived temperatures near the top of the section is likely to be real.

5.3. Comparisons With Published Regional Data

Relative Early Miocene warmth in Patagonia has been qualitatively recognized based on local changes in both the terrestrial and marine fossil biotas. Much of the early work was done before a robust chronostratigraphic

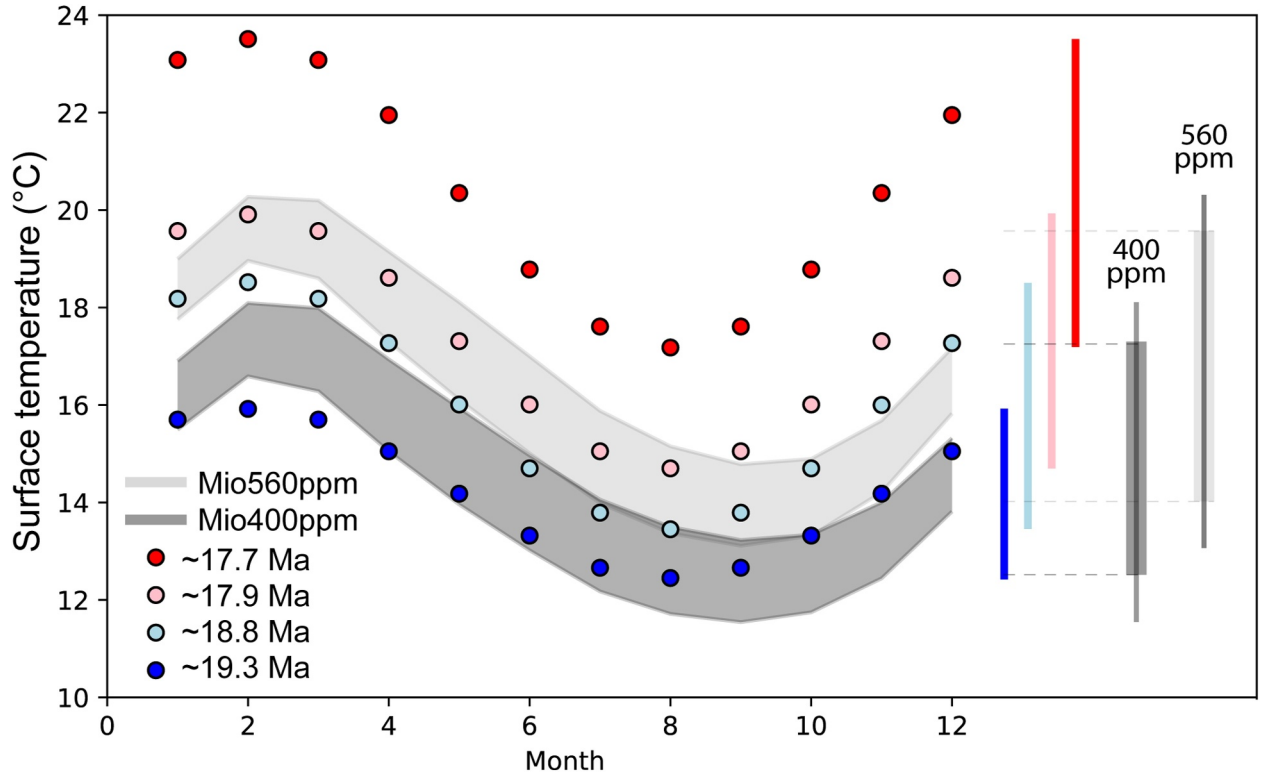

Figure 13. Modeled annual temperature cycle at 400 and 560 ppm in comparison to best-fit sinusoid monthly mean temperatures from fossil bivalves (δ^{18}Osw = −0.49). Model range integrates simulated temperatures from our locality and the immediately surrounding grid cells, to accommodate spatial heterogeneity. Bivalve data are generally well-described by the model and indicate warming consistent with rising pCO_2 through time, but the youngest (~17.7 Ma) sample is warmer and more seasonal than predicted by the model even at 560 ppm.

framework had been established, making a synthetic study of regional climate difficult. This limitation has now been rectified, and published interpretations can be plotted in a coherent framework along with our own data (Figure 13).

The paleobotanical record of Patagonia as a whole suggests that the middle Eocene to early Oligocene cooling trend marked by expansion of the *Nothofagus* forest reversed in the late Oligocene, and the region saw renewed expansion of megathermal (warm and humid) forest angiosperms and podocarps (Barreda & Palazzesi, 2007). Warm conditions continue into the Early Miocene, but with increasing aridity suggested by the limited appearance of grasses, xeric taxa, and sclerophyllous trees and the concomitant decrease in podocarps. Megathermal elements return again briefly in leading up to the MCO before cooling and drying in the Middle-Late Miocene (14–6 Ma), which transformed the Patagonian landscape to one more like today (Barreda & Palazzesi, 2007). This is supported by Miocene modeling work under high CO_2 scenarios (Acosta et al., 2022). In the Austral—Magallanes Basin specifically, late Oligocene warmth and humidity is inferred from palynomorph associations in the San Julián Formation at 23.53–22.77 Ma (Barreda, 2002, and references cited therein). Four hundred km to the north, in the Mazarredo and San Jorge basins (Figure 2), palynomorphs (dinoflagellate cysts, pollen, spores; Barreda & Palamarczuk, 2000) and mollusks (Barreda, 1997; del Río, 2021) similarly suggest humid and warm-temperate conditions around 20.9 Ma. Barreda and Palamarczuk (2000) and Barreda (2002) interpret the palynomorph record in the subsequent Burdigalian to indicate climatic "deterioration" (i.e., drying) in the San Jorge Basin (lower Chenque Formation from 19.6 to 15 Ma), the Mazarredo Basin (Mazarredo Formation, 20.5 Ma), and the Austral—Magallanes Basin (MLF from 19.36 to 17.73 Ma). This is the interval during which Barreda and Palazzesi (2007) recognize a short-lived advance of megathermal elements, suggesting a return to warmer conditions approaching the MCO.

The marine microfossil record of the Monte León Formation (Austral—Magallanes Basin) is consistent with fully marine conditions during the deposition of the Monte Entrada Member, followed by regressive deposits that

transition to shallow and potentially brackish, warmer water at the Monte Observación Member (Parras et al., 2020). The presence of mostly agglutinated foraminifera at the base of the MLF (Monte Entrada Member) (ca. 22.12 Ma) suggests the influx of cool, undersaturated subantarctic waters at the onset of transgression (Malumián & Náñez, 1991, 2011; Náñez et al., 2009). While nannoplankton assemblages from the unit exposed south of the Santa Cruz River record generally cool-water marine conditions throughout and beds directly underlying our Las Cuevas (LC; 17.91 Ma) horizon suggest upwelling of cold water during maximum transgression (Parras et al., 2020), miliolid foraminifera from the uppermost strata (our MO horizon; 17.69 Ma) point to warmth. For these beds, the authors suggest a delta front setting with fluctuating salinity (Parras et al., 2020). The inference of hyposaline waters differs from that derived from nannoplankton and inserts a note of caution as to whether the warmest temperatures from our MO horizon are associated with global/regional climate or instead reflect a facies change to shallower, more brackish water with increasing proximity to shore. As above (Section 5.2) however, mollusk paleoecology and the growth history of *Glycymerita* do not support an interpretation of low and fluctuating salinity in this horizon, at least in the setting in which *Glycymerita* were growing. It is possible, however, that *Glycymerita* shells living in adjacent deeper water were transported into more onshore facies during storms, explaining the presence of their marine traits in sediments that bear microfossils of a more coastal nature.

Recent work on the dinoflagellate assemblages of the Scotia Sea documents the disappearance of Antarctic cold-water endemics by the mid-Oligocene, the presence of temperate and low-nutrient assemblages in the MCO, and indicators of high-nutrient and sea-ice conditions in the colder Middle Miocene Climate Transition that followed ca. 14 Ma (Hoem et al., 2024). TEX_{86} data from ODP Site 696, in the northern Wedell Sea, suggest warm conditions (14°C) during the MCO (Hoem et al., 2023). The dinocyst assemblage from the Maurice Ewing Bank in the SW Atlantic suggests that the Subtropical Front moved north of that location in the Early Miocene (Hoem et al., 2024), but paleotemperature proxy data are not yet available from any Early Miocene deep-sea cores in the SW Atlantic.

The record of austral marine mollusks in Patagonia, so instrumental to Cenozoic biostratigraphy and biogeography in the region (del Río, 1990, 1997, 2000, 2004b, 2004c, 2021; del Río & Martínez, 2015; Martínez & del Río, 2002a, 2002b), has also proven useful for paleoclimate inference due to the thermal sensitivity of taxa. Changes in biogeographic affiliation over the Cenozoic allowed for the recognition of five major faunal associations that relate to differences in thermal regime (del Río, 2021). Like the paleobotanical record and marine vertebrate record, the Early Miocene molluscan assemblage of Patagonia (Austral—Magallanes, San Jorge and Mazarredo basins) contains a diagnostic suite of taxa that suggests temperatures warmer than today at the same latitudes but cooler than those inferred from Eocene and Middle Miocene associations (del Río, 2021). Key indicators of warm-temperate conditions are the presence of a much-reduced suite of cosmopolitan genera from tropical and warmest subtropical environments (*Arca, Barbatia, Crassatella, Trachycardium, Ficus, Conus, Borsonia, Liotia, Retizafra, Sveltia, Scalptia, Dalium*) and the survival of only a few Tethyan elements (e.g., *Parinomya, Limatula, Cucullaria, Darwinicardia, Eosolen, Bathytormus*), combined with the *en masse* arrival of subtropical Neogene Southern elements that make up nearly a quarter of the Early Miocene assemblage (del Río, 2021). The fauna is diverse, including also the appearance of up to 21 new endemic genera within the Pectinidae, Volutidae, Carditidae, Muricidae and Turridae. This Early Miocene fauna was largely replaced in the Middle Miocene by an assemblage characterized by the appearance of warm-water Caribbean (*Amusium, Nodipecten, Clementia, Torcula, Muracypraea,* and *Antinioche*) and tropical (*Profundimitra, Sconsia*) genera; only a few warm-temperate genera from the Early Miocene (*Sveltia, Ficus, Conus, Dalium*) persisted into the warmer MCO seas (del Río, 2021). The record of marine vertebrates in Patagonia similarly suggests temperate conditions, with neither tropical nor Magellanean (cold temperate) elements present in the early Miocene (Cione et al., 2011).

While climate inferences like these drawn from the changing distributions of very large numbers of taxa are likely robust, there is nevertheless some uncertainty associated with assuming taxonomic uniformitarianism to make climate inferences. The two surviving genera sampled here illustrate the issue: *Cucullaea* and *Retrotapes* both lived at the higher latitudes of Antarctica during the globally warm Eocene, inhabiting waters comparable in temperature to those we find in the (lower latitude) Early Miocene of southern Patagonia (Douglas et al., 2014; Ivany et al., 2008). *Cucullaea* has since tracked those temperatures to even lower latitudes today, consistent with the uniformitarian assumption, while evolution has enabled *Retrotapes* to adapt to the now-cooler conditions in Patagonia and remain in the area. Likewise, the cooccurrence of 4 species of penguin at the base of the early Miocene Gaiman Formation further north together with a diverse warm-temperate marine vertebrate fauna led

authors to conclude that these taxa, distinct from living genera, had adapted to the warmer waters like those in the Galapagos today, and did not reflect the presence of episodic cool-water habitats or mixing of fossils from an earlier (unpreserved) cool interval during transgression, as might be inferred from a uniformitarian assumption (Cione et al., 2011).

Temperature estimates based on the isotope values of mollusk shells offer an important quantitative, independent constraint on regional paleoclimate that circumvents uniformitarian assumptions. Published isotope-based paleotemperature estimates from Patagonia were very few until now. Two earlier studies used the shells of the oyster *Crassostrea hatcheri* from the correlative Estancia 25 de Mayo Formation, exposed on the south side of Lago Argentino in the southwestern sector of the Austral—Magallanes Basin (Figure 1) and at a slightly (<1°) higher paleolatitude, for paleoclimate inference (Casadío et al., 2000; Cuitiño et al., 2013). The general transgressive-regressive facies progression here is comparable to that seen in the MLF, but the time encompassed by marine sedimentation is much restricted given its more inboard position - the lower Quién Sabe Member of the Estancia 25 de Mayo Formation has been dated at ca. 20–19.3 Ma, and the base of the overlying Santa Cruz Formation here is 18.8 Ma (Cuitiño et al., 2012, 2013) (Figure 2). Lithostratigraphic contacts, particularly the transition from marine to continental deposition, are therefore time transgressive. $\delta^{18}O$ values from the translucent layers of *C. hatcheri* shells carefully screened for diagenesis are roughly 0.5–1.0‰ lower than our data from the MLF (Cuitiño et al., 2013), and using the same $\delta^{18}O$ value for seawater of −0.49‰ with the Erez and Luz (1983) paleotemperature equation for calcite yields temperatures averaging around 17.5°C. The lack of any stratigraphic trend in their isotope data is consistent with that observed in the (>18 Ma) Darwin Section of the MLF reported here, and if so, their temperatures are slightly warmer than ours (Figure 14). Shells of *C. hatcheri* are associated with a diverse marine fauna, but their geographic position closer to the rising Andes and the intercalation of monospecific beds of *C. orbignyi* with much more negative isotope values suggest the potential for freshwater mixing in this setting (Cuitiño et al., 2013). Accretionary data from a single *C. hatcheri* shell from each study (Casadío et al., 2000; Cuitiño et al., 2013) yield winter temperatures (14.3 and 13.4°C) that compare reasonably well to our Darwin section data, but summer temperatures (21.1 and 21.2°C, from the first half of shell ontogeny only, where the annual cycle is readily apparent) are warmer (compare to Figures 7 and 10). Given the more proximal facies of the Estancia 25 de Mayo Fm., water $\delta^{18}O$ values particularly in summer could be influenced by freshwater discharge, yielding calculated paleotemperatures that are artificially warm.

Overall then, changes in biotic assemblages and the limited existing geochemical proxy data point to warm-temperate conditions in the Early Miocene of southern Patagonia, with warming and drying into the MCO (Figure 14). Our stable isotope data from MLF mollusks provide substantial quantitative support for this inference, constrain the seasonal range and extremes through the section, and point to the likelihood of warming into the MCO beginning around 18 Ma, brought about particularly by increasingly warm summers.

5.4. Insights From Paleoclimate Modeling

Comparisons of best-fit seasonally resolved proxy data with predictions from a climate model provide important groundtruthing information with which to evaluate model performance and place constraints on fundamental aspects of the climate system, such as climate sensitivity, pCO_2, and the degree of polar amplification of warming (Lunt et al., 2024). The dearth of samples from the SE Pacific and SW Atlantic around South America (Burls et al., 2021; Hoem et al., 2024) highlights the importance of our data from Patagonia in offering constraints on conditions in the run-up to the MCO. All simulation files and the subset of MioMIP data discussed below are available from the Zenodo repository using the link in the Data Availability Statement at the end of this paper.

Early Miocene proxy data from ca. 19 Ma agree well with Miocene climate simulations conducted with a 400 ppm atmospheric CO_2 concentration, consistent with global proxy data for pCO_2 at this time ($CenCO_2PIP$ et al., 2023) and supporting cooler conditions before the MCO (Figures 11c and 11d). Approaching the MCO (<18 Ma), proxy data match better with Miocene climate simulation under a 560 ppm CO_2 atmosphere (Figures 11a and 11b), suggesting that the degree of warming leading up to the MCO is aligned with a global CO_2 increase of the same magnitude suggested by pCO_2 proxy data ($CenCO_2PIP$ et al., 2023). Note that general agreement of our proxy data with the coupled climate model simulations in the 400–560 ppm range, in combination with data from the southern hemisphere Pacific and Indian Ocean sectors (Figure 15), suggests that the iCESM1.2 model is able to capture the degree of warmth indicated by the Early Middle Miocene proxy data from the Southern Hemisphere better than the earlier multi-model ensemble Deep-MIP Miocene (Burls et al., 2021). If $\delta^{18}Osw$ values are found

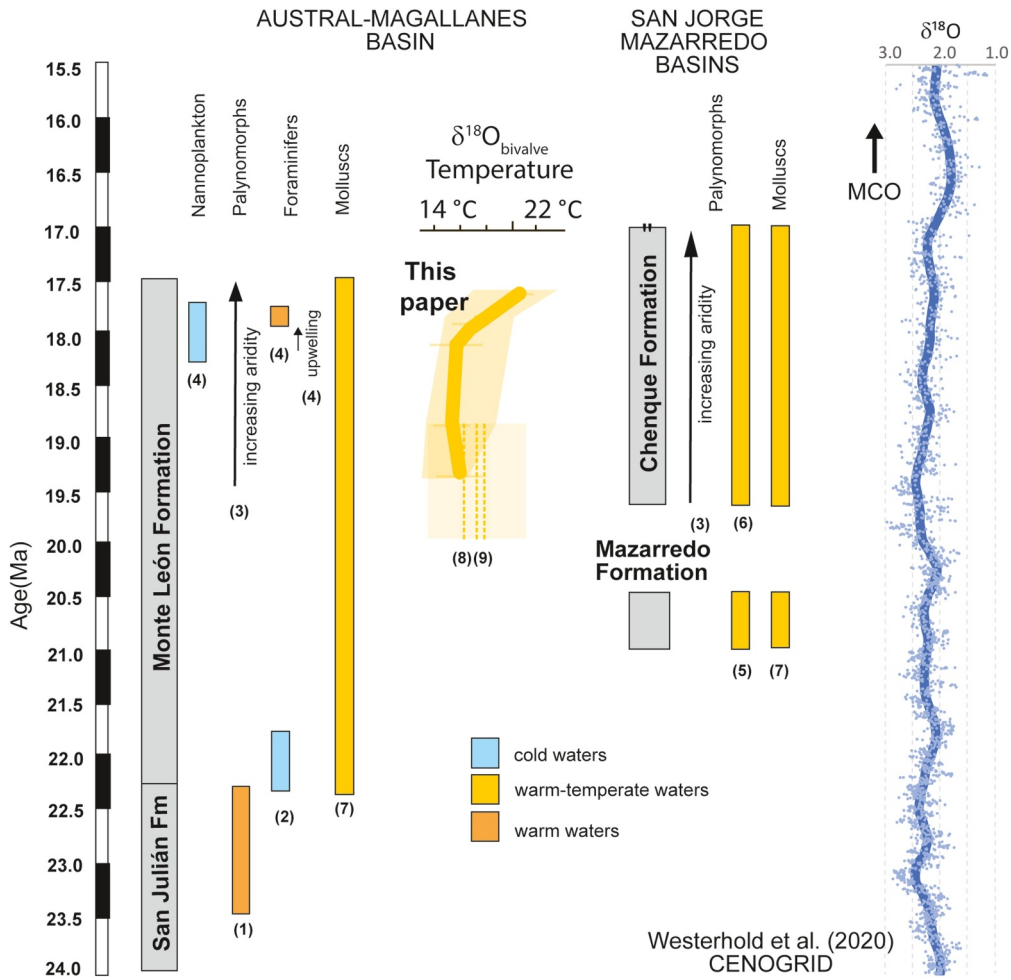

Figure 14. Synthesis of paleoclimatic inferences for southern Patagonia based upon assemblages of marine and terrestrial palynomorphs, foraminifers, nannoplankton, and mollusks, plotted alongside $\delta^{18}O$-based temperature calculations from this paper, Casadío et al. (2000), and Cuitiño et al. (2013), and showing the benthic foraminiferal $\delta^{18}O$ record from Westerhold et al. (2020) for comparison. Miocene Climatic Optimum begins at ~17 Ma. References are as follows: (1) Barreda (1997); (2) Malumián and Náñez (1991), Náñez et al. (2009); (3) Barreda (2002); (4) Parras et al. (2020); (5) Barreda and Palamarczuk (2000); (6) Barreda and Palazzesi (2007); (7) del Río (2021); (8) Casadío et al. (2000) and (9) Cuitiño et al. (2013), from the Estancia 25 de Mayo Formation (a proximal unit with potential freshwater influence; age uncertainty indicated by dashed vertical lines). Ages of the Monte León and San Julián Formation from Parras et al. (2012), Mazarredo Formation from del Río et al. (2022), lower section of the Chenque Formation from Cuitiño et al. (2015a, 2015b) and del Río et al. (2022), and Estancia 25 de Mayo Formation from Cuitiño et al. (2013).

to be significantly more positive, however, as suggested by Meckler et al. (2022), calculated temperatures would remain well out of reach of model predictions, as is the case with northern mid-high-latitude data derived from organic proxies (Burls et al., 2021).

For our uppermost horizon, proxy-derived temperatures are ~4°C warmer and a degree more seasonal than models with realistic pCO_2 (Figures 11b and 13). Is this proxy-model mismatch informative, and what might it point to? As discussed already, the likelihood of mixing with isotopically negative fresh water from runoff is low in this case, given the stenohaline paleoecology and long life history of the taxon from which the data come and the consistency of winter and summer isotope values over at least 11 years of growth. Underestimation of pCO_2 and/or underestimation of temperature by the model in the approach to the MCO is another possibility that could account for the offset. Our proxy data from these ~17.75 Ma samples show some agreement with samples at the same latitude from IODP Site 1171, potentially indicating that the model is slightly underestimating high-latitude temperatures overall (Figure 11b). However, nearby polar SST Sites (AND-2A) suggest cooler temperatures than the model (by 2–3°C, Figure 11b), and the best estimates for pCO_2 based on the geologic record suggest values around 500 ppm at this

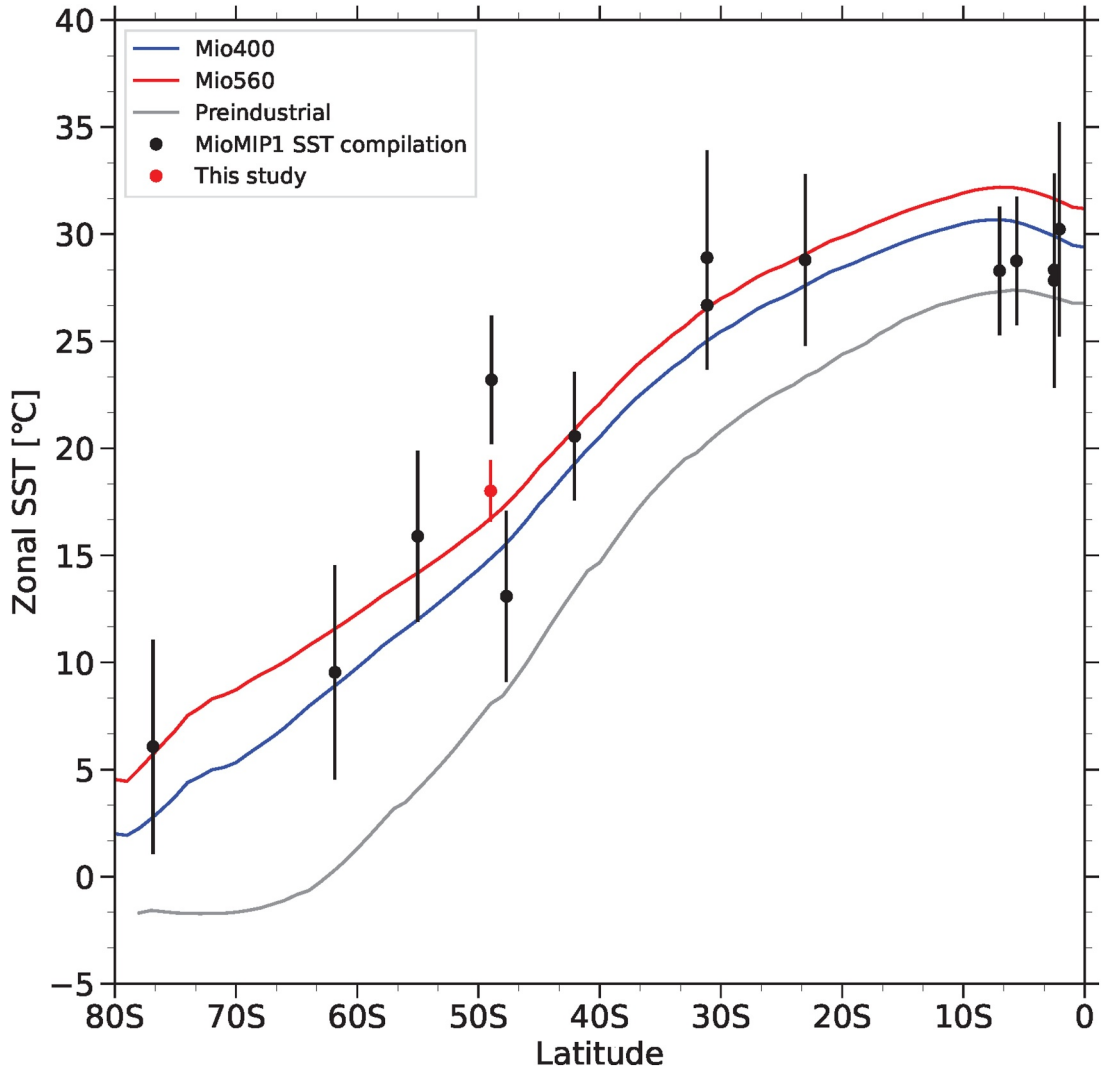

Figure 15. Zonal mean temperatures produced by the Miocene iCESM at 400 and 560 ppm and the Preindustrial simulations in the Southern hemisphere. Proxy data (mean sea-surface temperature values from 17 Ma samples) from this study (red symbol) are compared to those from the MioMIP compilation (black symbols) of Burls et al. (2021) for the Southern hemisphere. Plotted MioMIP data come almost exclusively from the SW Pacific Ocean and around South Africa.

time (CenCO$_2$PIP et al., 2023), so we refrain from speculating that a substantially higher CO_2 configuration is more appropriate. Models of warm-climate scenarios, including the MCO, often struggle to capture the degree of high-latitude warming, for example, the shallow Northern Hemisphere equator to pole temperature gradient, indicated by the data without overheating the tropics (Burls et al., 2021; Goldner et al., 2014). This small underestimation of Patagonian proxy temperatures by models that faithfully reproduce tropical temperatures (Acosta, Burls, Pound, Bradshaw, McCoy, et al., 2024; Acosta et al., 2022; Gaskell et al., 2022), particularly as climate warms in the run-up to the MCO, could relate to this still-unresolved phenomenon.

Another option is that the model might not be capturing some aspect of regional heterogeneity experienced by the Patagonian shelf. Mean temperature and seasonal extremes in our uppermost horizon are warmer than suggested by the model at 560 ppm, a difference that appears to be due in the model primarily to the intrusion of cool water from the Southern Ocean (the Malvinas/Falkland current, a northern offshoot of the Antarctic Circumpolar Current (ACC)) (Figure 12). Warmer temperatures suggest a weaker Malvinas current and/or ocean transport from a warmer Southern Ocean at this time. The similarity of our data to proxy SSTs from IODP 1171 suggests that a warmer Southern Ocean overall is likely (Figure 11). Our Miocene simulations contain a fully open Drake Passage with strong ACC and Malvinas currents. There is longstanding debate about when this configuration was

attained. A steep temperature gradient between Antarctica and subantarctic regions by the Middle Miocene suggests a strong ACC by that time (Hoem et al., 2023), but if the ACC and hence Malvinas current were not yet well developed in the early Miocene, our model would overestimate its cooling impact in the region. If the more positive δ^{18}Osw values of Meckler et al. (2022) find support in future work, then our proxy temperatures will be even more strongly underestimated by the model.

Seasonal proxy-model comparisons overall exhibit good agreement with the model (Figure 13), particularly if data from the oldest shell are indeed truncated by cessation of growth in the summer. Again though, data from the uppermost horizon are out of step, yielding a seasonal range somewhat higher than the model. In the region today, seasonal range in SSTs is higher than the zonal mean (Hirahara et al., 2014) due to seasonal oscillation in the confluence of the warm Brazil current from the north and the cold Malvinas current from the south (Wainer et al., 2000). This oscillation is evident in our model results (Figure 12), reflecting the modeled open Drake Passage and full Malvinas current. As pointed out by Judd et al. (2019) however, changes in the configuration of the Drake Passage could adjust the flow of the Malvinas current, changing the properties of the confluence and hence the seasonal range experienced. To the degree that the proxy-model offsets in mean temperature and seasonal range are significant, albeit small, they could reflect real spatial heterogeneity due to differences in how the Drake Passage affects temperatures in the model versus Early Miocene Patagonia.

A synthesis of Miocene climate modeling efforts demonstrates that pCO_2 is the dominant factor determining the degree of global warmth, but that paleogeography and ice volume can adjust mean global temperature by up to 2°C and have stronger regional effects (Burls et al., 2021). If paleogeography is responsible for the small degree of mismatch between Early Miocene Patagonian data and the climate model, the most obvious source of uncertainty in this region at this time is the configuration of Drake Passage, although changes in the Panama and Mesopotamian gateways also affect circulation and heat distribution during this window of time (e.g., Bialik et al., 2019; von der Heydt and Dijkstra, 2006; Yang et al., 2014) and might contribute, for example, to the offset between northern Atlantic and Pacific paleotemperatures (Nirenberg and Herbert, 2025). There is now growing consensus that a fully open Drake Passage, enabling consistent deepwater ACC circulation, was not established until sometime later in the Miocene (Dalziel et al., 2013; Evangelinos et al., 2024; Hoem et al., 2023; Pérez et al., 2019), despite an intermittent deep connection since the mid-late Oligocene (Hodel et al., 2021; Lyle et al., 2007). Tectonism in Tierra del Fuego and the widening Scotia Sea generated small continental blocks that variably impeded eastward flow of the ACC though the widening Drake Passage until sometime in the early Neogene (van de Lagemaat et al., 2021). Lagabrielle et al. (2009) link early Miocene spreading in the Scotia Sea to shallowing and constriction of the Drake Passage and indeed the transgression in the Austral—Magallanes Basin that gives rise to the Monte León Formation. Recently published dinocyst assemblages from the Scotia Sea and northwest Weddell Sea support increasing flow through the Drake beginning in the late Oligocene, restricting subpolar gyre circulation and pushing the sub-tropical front north by the early Miocene, but that the Subantarctic front remained in the Scotia Sea until after the MCO (Hoem et al., 2024). This leaves open the possibility that changes in gateway configuration drove changes in circulation and regional climate that are superimposed on the global backdrop of MCO warming arising from changes in pCO_2. Southern Patagonia is well positioned to record changes in the strength of ACC flow and related regional climate effects as Drake Passage attains its full and open configuration.

Simulations with a fully open Drake Passage by Vincze et al. (2021), Toumoulin et al. (2020) and Sauermilch et al. (2021) all indicate not only a cooler Southern Ocean, but also significantly warmer temperatures on the Patagonian coastline in comparison to configurations with a closed Drake Passage. Stronger ACC flow results in weakening and restriction of the subpolar gyres, trapping cold water farther south, and is coupled to a stronger Malvinas Current, driving an increase in seasonal range along the SE Patagonian coast. Development of a gap in the North Scotia Ridge ca. 18 Ma (Eagles and Jokat, 2014), evidenced by initiation of deepwater sedimentation in the Argentine Basin around 17 Ma (Ghiglione et al., 2016), suggests northern ACC water began entering the south Atlantic as the Malvinas Current at about this time, and contourite deposits off the coast suggest a dynamic flow regime that Unland and colleagues (2024) link to initiation of the Brazil-Malvinas confluence. The shift toward warmer and more seasonal temperatures in the MLF beginning around 18 Ma might record this attainment of more open flow through the Drake Passage (warming SE Patagonia) and establishment of the seasonally oscillating confluence of the Brazil-Malvinas currents (increasing the seasonal temperature range). Whether or not these phenomena are in fact recorded in the sediments of the Austral—Magallanes Basin and superimposed on the impacts of changing pCO_2 is something that could be better addressed with (a) expanded spatio-temporal

coverage of seasonally resolved isotope data from Patagonian fossil mollusks, and (b) a climate model with finer spatial resolution to better simulate the impact of changes in gateway configuration on regional circulation and climate, and (c) comparison with climate model simulations using a closed Drake Passage.

6. Conclusions

Mean SST proxy data from Monte León Formation bivalves are generally well-predicted by climate models simulating pCO_2 between 400 and 560 ppm, consistent with paleoCO_2 proxy data for this time and supporting CO_2 as the primary control on Early Miocene paleoclimate conditions in Patagonia approaching the MCO. Nevertheless, the fact that Early Miocene Patagonian paleotemperatures (~15–20°C) were so much warmer than today (6–10°C), despite similar estimates for pCO2, emphasizes that other factors, such as ice albedo (Burls et al., 2021), gateway paleogeography (Evangelinos et al., 2024; Lagabrielle et al., 2009), and/or ocean circulation (Herold et al., 2012), were augmenting Miocene warmth. Given the dearth of proxy data from the southern hemisphere, particularly in the Atlantic Ocean, our records provide important new constraints from a key climatically sensitive region that, in combination with climate models, can help resolve these remaining uncertainties. Data from SE Patagonia indicate warming and increasing seasonality through the Burdigalian in the lead-up to the MCO, a pattern not only consistent with rising pCO_2 approaching the MCO, but also with increasingly uninterrupted flow through the Drake Passage and development of a strong Malvinas current. The degree to which the latter is true will point to a continuing role for Drake Passage gateway configuration affecting climate during the Miocene.

Data Availability Statement

Early Miocene fossil data used for proxy-model comparison and output for early to-Middle Miocene simulations with sea surface temperature are available from the Zenodo repository (Ivany and Acosta, 2025).

Acknowledgments

Thanks to Natalie Burls and Tripti Bhattacharya for assistance and discussion and to Ana Parras (University of La Pampa, Argentina) for stratigraphic discussion. Beatriz Aguirre Urreta and Marian Tanuz, curators of the collection at the University of Buenos Aires, are gratefully acknowledged for their help. We thank Bruce Wilkinson for computing best-fit growth curves. Members of the PaleoX Research Group at SU and two anonymous reviewers offered much helpful feedback. C. del Río and S. Raigemborn acknowledge support from Grant PIP-CONICET 391. Field collections were facilitated by earlier Grants PIP–CONICET 1649 and PICT-ANPCyT 1839 and PICT-ANPCyT 57 to C. del Río. Acosta acknowledges support from NSF AGS-1844380 and NSF EAR-2303417. This work was supported in part by a Sepkoski grant from the Paleontological Society to M. Alvarez, and by funds from Syracuse University's Department of Earth and Environmental Sciences and the University of Michigan Stable Isotope Lab.

References

Acosta, R. P., Burls, N. J., Pound, M. J., Bradshaw, C. D., De Boer, A. M., Herold, N., et al. (2024). A model-data comparison of the hydrological response to Miocene warmth: Leveraging the MioMIP1 opportunistic multi-model ensemble. *Paleoceanography and Paleoclimatology*, *39*(1), e2023PA004726. https://doi.org/10.1029/2023pa004726

Acosta, R. P., Burls, N. J., Pound, M. J., Bradshaw, C. D., McCoy, J., Gibson, M., et al. (2024). Climate conundrum: A wet or dry European and northern African climate during the middle Miocene. *Geophysical Research Letters*, *51*(21), e2024GL109499. https://doi.org/10.1029/2024gl109499

Acosta, R. P., Ladant, J. B., Zhu, J., & Poulsen, C. J. (2022). Evolution of the Atlantic Intertropical Convergence Zone, and the South American and African monsoons over the past 95-Myr and their impact on the tropical rainforests. *Paleoceanography and Paleoclimatology*, *37*(7), e2021PA004383. https://doi.org/10.1029/2021pa004383

Alvarez, M., del Río, C. J., & Martínez, S. (2020). Revision of the subfamily Pitarinae Stewart, 1930 (*Eucallista* Dall, 1902; *Austrocallista* Erdmann & Morra, 1985; *Proteopitar* nov. Gen.) from Cenozoic southern South America: Systematic and Phylogenetic analyses. *Journal of Systematic Paleontology*, *18*(5), 433–460. https://doi.org/10.1017/jpa.2020.30

Barreda, V. (1997). Palinoestratigrafía de la Formación San Julián en el área de Playa La Mina (Provincia de Santa Cruz), Oligoceno de la Cuenca Austral. *Ameghiniana*, *34*, 283–294.

Barreda, V. (2002). Palinofloras Cenozoicas. In M. Haller (Ed.), *Geología y Recursos Naturales de Santa Cruz. 15 Congreso Geológico Argentino* (pp. 545–567). El Calafate.

Barreda, V., & Palamarczuk, S. (2000). Palinoestratigrafía de depósitos del Oligoceno tardío-Mioceno en el área sur del Golfo San Jorge, provincia de Santa Cruz. *Ameghiniana*, *37*(1), 103–117.

Barreda, V., & Palazzesi, L. (2007). Patagonian vegetation turnovers during the Paleogene-early Neogene: Origin of arid-adapted floras. *The Botanical Review*, *73*(1), 31–50. https://doi.org/10.1663/0006-8101(2007)73[31:pvtdtp]2.0.co;2

Bellosi, E. S. (1990). Formación Chenque: Registro de la transgresión *Patagoniana* (Terciario medio) de la cuenca de San Jorge, Argentina. *11° Congreso Geológico Argentino*, *2*, 57–60.

Bertels, A. (1970). Sobre el "Piso Patagoniano" y la representación de la época del Oligoceno en Patagonia austral, República Argentina. *Revista de la Asociación Geológica Argentina*, *25*(4), 495–501.

Bialik, O. M., Frank, M., Betzler, C., Zammit, R., & Waldmann, N. D. (2019). Two-step closure of the Miocene Indian Ocean Gateway to the Mediterranean. *Scientific Reports*, *9*(1), 8842. https://doi.org/10.1038/s41598-019-45308-7

Brady, E., Stevenson, S., Bailey, D., Liu, Z., Noone, D., Nusbaumer, J., et al. (2019). The connected isotopic water cycle in the Community Earth System Model version 1. *Journal of Advances in Modeling Earth Systems*, *11*(8), 2547–2566. https://doi.org/10.1029/2019ms001663

Buick, D. P. (2009). *The rise and fall of the Cucullaeidae: Exploring transitions in species richness, geographic range, morphology, and ecology in a relict bivalve family*. PhD Dissertation (p. 483). Univ. of Cincinnati.

Burls, N. J., Bradshaw, C. D., De Boer, A. M., Herold, N., Huber, M., Pound, M., et al. (2021). Simulating Miocene warmth: Insights from an opportunistic multi-model ensemble (MioMIP1). *Paleoceanography and Paleoclimatology*, *36*(5), e2020PA004054. https://doi.org/10.1029/2020pa004054

Casadío, S., Feldmann, R. M., & Foland, K. A. (2000). 40Ar/39Ar age and oxygen isotope temperature of the Centinela Formation, southwestern Argentina: An Eocene age for crustacean-rich "Patagonian" beds. *Journal of South American Earth Sciences*, *13*(1–2), 123–132. https://doi.org/10.1016/s0895-9811(00)00013-4

CenCO$_2$PIP—The Cenozoic CO$_2$ Proxy Integration Project Consortium, Hönisch, B., Royer, D. L., Breecker, D. O., Polissar, J., Bowen, G. J., et al. (2023). Toward a Cenozoic history of atmospheric CO$_2$. *Science*, *382*(6675), eadi5177. https://doi.org/10.1126/science.adi5177

Chiesa, J. O., & Camacho, H. H. (1995). Litoestratigrafía del Paleógeno marino en el noroeste de la provincia de Santa Cruz, Argentina. *Monografía de la Academia Nacionalde Ciencias Exactas Físicas y Natutrales, Buenos Aires*, *11*, 9–15.

Cione, A. L., Cozzuol, M. A., Dozo, M. T., & Acosta Hospitaleche, C. (2011). Marine vertebrate assemblages in the southwest Atlantic during the Miocene. *Biological Journal of the Linnean Society*, *103*(2), 423–440. https://doi.org/10.1111/j.1095-8312.2011.01685.x

Cochran, J. K., Kallenberg, K., Landman, N. H., Harries, P. J., Weinreb, D., Turekian, K. K., et al. (2010). Effect of diagenesis on the Sr, O, and C isotope composition of late Cretaceous mollusks from the western interior seaway of North America. *American Journal of Science*, *310*(2), 69–88. https://doi.org/10.2475/02.2010.01

Codignotto, J. O., & Malumián, N. (1981). Geología de la región al Norte del paralelo 54∘ S. de la Isla Grande de Tierra del Fuego. *Revista de la Asociación Geológica Argentina*, *36*(1), 44–88.

Cuitiño, J. I., Pimentel, M. M., Ventura Santos, R., & Scasso, R. A. (2012). High resolution isotopic ages for the early Miocene "Patagoniense" transgression in southwest Patagonia: Stratigraphic implications. *Journal of South American Earth Sciences*, *38*, 110–122. https://doi.org/10.1016/j.jsames.2012.06.008

Cuitiño, J. I., & Scasso, R. A. (2010). Sedimentología y paleoambientes del Patagoniano y su transición a la Formación Santa Cruz al sur del Lago Argentino, Patagonia austral. *Revista de la Asociación Geológica Argentina*, *66*(3), 406–417.

Cuitiño, J. I., Scasso, R. A., Ventura Santos, R., & Mancini, L. H. (2015b). Sr ages for the Chenque Formation in the Comodoro Rivadavia región (Golfo San Jorge basin, Argentina): Stratigraphic implications. *Latin American Journal of Sedimentology and Basin Analysis*, *22*(1), 3–12.

Cuitiño, J. I., Ventura Santos, R., Alonso Muruaga, P. J., & Scasso, R. A. (2015a). Sr-stratigraphy and sedimentary evolution of Early Miocene marine foreland deposits in the northern Austral (Magallanes) Basin, Argentina. *Andean Geology*, *42*(3), 364–385.

Cuitiño, J. I., Ventura Santos, R., & Scasso, R. A. (2013). Insights into the distribution of shallow-marine to estuarine Early Miocene oysters from Southwestern Patagonia: Sedimentologic and stable isotope constraints. *PALAIOS*, *28*, 583–598.

Dalziel, I. W. D., Lawver, L. A., Pearce, J. A., Barker, P. F., Hastie, A. R., Barfod, D. N., et al. (2013). A potential barrier to deep Antarctic circumpolar flow until the Late Miocene? *Geology*, *41*(9), 947–950. https://doi.org/10.1130/g34352.1

Darwin, C. (1846). Geological observations on the volcanics Islands and parts of South America visited during the Voyage of H.M.S. 1–548.

Dávila, F. M., Lithgow-Bertelloni, C., Martina, F., Ávila, P., Nóbile, J., Collo, G., et al. (2018). Mantle influence on Andean and pre-Andean topography. *The Evolution of the Chilean-Argentinean Andes*, 363–385. https://doi.org/10.1007/978-3-319-67774-3_15

del Río, C. J. (1990). Composición, origen y significado paleoclimático de la malacofauna "Entrerriense" (Mioceno medio) de la Argentina. *Anales de la Academia Nacional de Ciencias Exactas, Físicas y Naturales, Buenos Aires*, *42*, 207–226.

del Río, C. J. (1995). The genus Swiftopecten Hertlein, 1935 (Bivalvia: Pectinidae) in the Tertiary of Southern South America. *Journal of Paleontology*, *69*(6), 1054–1059. https://doi.org/10.1017/S0022336000038038

del Río, C. J. (1997). Cenozoic biogeographic history of the eurythermal genus Retrotapes New Genus (Subfamily Tapetinae) from Southern South America and Antarctica. *Nautilus*, *110*(3), 77–93. https://doi.org/10.5962/bhl.part.3573

del Río, C. J. (2000). Malacofaunas de las formaciones Paraná y Puerto Madryn (Mioceno marino, Argentina): Su origen, composición y significado bioestratigráfico. In F. G. Aceñolaza & R. Herbest (Eds.), *El Neógeno de Argentina* (Vol. 14, pp. 77–101). INSUGEO, Serie de Correlación Geológica.

del Río, C. J. (2004a). Revision of the large Neogene pectinids (Mollusca: Bivalvia) of Eastern Santa Cruz and Chubut Provinces (Patagonia - Argentina). *Journal of Paleontology*, *78*(4), 690–699. https://doi.org/10.1666/0022-3360(2004)0782.0.CO;2

del Río, C. J. (2004b). Tertiary marine molluscan assemblages of eastern Patagonia (Argentina): A biostratigraphic analysis. *Journal of Paleontology*, *78*(4), 1097–1122. https://doi.org/10.1666/0022-3360(2004)078<1097:tmmaoe>2.0.co;2

del Río, C. J. (2004c). Relaciones biogeográficas entre los moluscos el Miocen tardíos y Recientes del Atántico Sudoccidental. In F. G. Aceñolaza (Ed.), *Temas dela Biodiversidad del litoral fluvial argentino* (Vol. 12, pp. 39–44). INSUGEO, Miscelánea.

del Río, C. J. (2006). El género Nodipecten Dall (Bivalvia - Pectinidae) en el Neógeno de la Patagonia (Argentina). *Ameghiniana*, *43*(4), 745–756.

del Río, C. J. (2021). Paleoclimate and changing composition of the Paleogene-Neogene shallow molluscan assemblages of Patagonia. *Journal of South American Earth Sciences*, *108*, 103209. https://doi.org/10.1016/j.jsames.2021.103209

del Río, C. J., Bellosi, E. S., McArthur, J. M., & Thirlwall, M. F. (2022). Early Miocene Sr-geochronology of *Patagoniense* marine units from southern Argentina: Implications for molluscan assemblages and interbasinal correlation. *Journal of South American Earth Sciences*, *120*, 104097. https://doi.org/10.1016/j.jsames.2022.104097

del Río, C. J., & Camacho, H. H. (1998). Tertiary Nuculoids and arcoids of eastern Patagonia (Argentina). *Palaeontographica, Abteilung A, Band*, *250*(1–3), 47–88. https://doi.org/10.1127/pala/250/1998/47

del Río, C. J., & Martínez, S. A. (2006). The family Volutidae in the Tertiary of Argentina (Mollusca-Gastropoda). *Journal of Paleontology*, *80*(5), 919–945. https://doi.org/10.1666/0022-3360(2006)80[919:TFVMIT]2.0.CO;2

del Río, C. J., & Martínez, S. A. (2015). Paleobiogeography of the Danian molluscan assemblages of Patagonia (Argentina). *Palaeogeography, Palaeoclimatology, Palaeoecology*, *417*, 274–292. https://doi.org/10.1016/j.palaeo.2014.10.006

Douglas, P. M., Affek, H. P., Ivany, L. C., Houben, A. J., Sijp, W. P., Sluijs, A., et al. (2014). Pronounced zonal heterogeneity in Eocene southern high-latitude sea surface temperatures. *Proceedings of the National Academy of Sciences*, *111*(18), 6582–6587. https://doi.org/10.1073/pnas.1321441111

Dunca, E., Mutvei, H., Göransson, P., Mörth, C. M., Schöne, B. R., Whitehouse, M. J., et al. (2009). Using ocean quahog (*Arctica islandica*) shells to reconstruct palaeoenvironment in Öresund, Kattegat and Skagerrak, Sweden. *International Journal of Earth Sciences*, *98*, 3–17.

Eagles, G., & Jokat, W. (2014). Tectonic reconstructions for paleobathymetry in Drake Passage. *Tectonophysics*, *611*, 28–50. https://doi.org/10.1016/j.tecto.2013.11.021

Erez, J., & Luz, B. (1983). Experimental paleotemperature equation for planktonic foraminifera. *Geochimica et Cosmochimica Acta*, *47*(6), 1025–1031. https://doi.org/10.1016/0016-7037(83)90232-6

Evangelinos, D., Etourneau, J., van de Flierdt, T., Crosta, X., Jeandel, C., Flores, J. A., et al. (2024). Late Miocene onset of the modern Antarctic circumpolar current. *Nature Geoscience*, *17*(2), 165–170. https://doi.org/10.1038/s41561-023-01356-3

Evans, D. (2021). Deep heat: Proxies, Miocene ice, and an end in sight for paleoclimate paradoxes? *Paleoceanography and Paleoclimatology*, *36*(3), e2020PA004174. https://doi.org/10.1029/2020pa004174

Gaskell, D. E., Huber, M., O'Brien, C. L., Inglis, G. N., Acosta, R. P., Poulsen, C. J., & Hull, P. M. (2022). The latitudinal temperature gradient and its climate dependence as inferred from foraminiferal $\delta^{18}O$ over the past 95 million years. *Proceedings of the National Academy of Sciences*, *119*(11), e2111332119. https://doi.org/10.1073/pnas.2111332119

Gasson, E., DeConto, R. M., Pollard, D., & Levy, R. H. (2016). Dynamic Antarctic ice sheet during the early to mid-Miocene. *Proceedings of the National Academy of Sciences*, *113*(13), 3459–3464. https://doi.org/10.1073/pnas.1516130113

Ghiglione, M. C., Sue, C., Ramos, M. E., Tobal, J. E., & Gallardo, R. E. (2016). The relation between Neogene denudation of the southernmost Andes and sedimentation in the offshore Argentine and Malvinas Basins during the opening of the Drake Passage. *Geodynamic Evolution of the Southernmost Andes: Connections with the Scotia Arc*, 109–135. https://doi.org/10.1007/978-3-319-39727-6_5

Goldner, A., Herold, N., & Huber, M. (2014). The challenge of simulating the warmth of the mid-Miocene climatic optimum in CESM1. *Climate of the Past*, *10*(2), 523–536. https://doi.org/10.5194/cp-10-523-2014

Goodwin, D. H., Schone, B. R., & Dettman, D. L. (2003). Resolution and fidelity of oxygen isotopes as paleotemperature proxies in bivalve mollusk shells: Models and observations. *PALAIOS*, *18*(2), 110–125. https://doi.org/10.1669/0883-1351(2003)18<110:rafooi>2.0.co;2

Griffin, M., & Pastorino, G. (2005). The genus *Trophon* Monfort, 1810 (Gastropoda: Muricidae) in the Tertiary of Patagonia. *Journal of Paleontology*, *79*(2), 296–311. https://doi.org/10.1666/0022-3360(2005)079<0296:TGTMGM>2.0.CO;2

Griffin, M., & Pastorino, G. (2013). Cenozoic Ampullinidae and Naticidae (Mollusca, Gastropoda) from Patagonia, Argentina. *Journal of Paleontology*, *87*(3), 502–525. https://doi.org/10.1666/12-148.1

Grossman, E. L., & Ku, T. L. (1986). Oxygen and carbon isotope fractionation in biogenic aragonite: Temperature effects. *Chemical Geology: Isotope Geoscience section*, *59*, 59–74. https://doi.org/10.1016/0168-9622(86)90057-6

Halberstadt, A. R. W., Chorley, H., Levy, R. H., Naish, T., DeConto, R. M., Gasson, E., & Kowalewski, D. E. (2021). CO_2 and tectonic controls on Antarctic climate and ice-sheet evolution in the mid-Miocene. *Earth and Planetary Science Letters*, *564*, 116908. https://doi.org/10.1016/j.epsl.2021.116908

Herbert, T. D., Dalton, C. A., Liu, Z., Salazar, A., Si, W., & Wilson, D. S. (2022). Tectonic degassing drove global temperature trends since 20 Ma. *Science*, *377*(6601), 116–119. https://doi.org/10.1126/science.abl4353

Herold, N., Huber, M., Müller, R. D., & Seton, M. (2012). Modeling the Miocene climatic optimum: Ocean circulation. *Paleoceanography*, *27*(1). https://doi.org/10.1029/2010pa002041

Hirahara, S., Ishii, M., & Fukuda, Y. (2014). Centennial-scale sea surface temperature analysis and its uncertainty. *Journal of Climate*, *27*(1), 57–75. https://doi.org/10.1175/JCLI-D-12-00837.1

Hodel, F., Grespan, R., de Rafélis, M., Dera, G., Lezin, C., Nardin, E., et al. (2021). Drake Passage gateway opening and Antarctic Circumpolar Current onset 31 Ma ago: The message of foraminifera and reconsideration of the Neodymium isotope record. *Chemical Geology*, *570*, 120171. https://doi.org/10.1016/j.chemgeo.2021.120171

Hoem, F. S., López-Quirós, A., Van De Lagemaat, S., Etourneau, J., Sicre, M. A., Escutia, C., et al. (2023). Late Cenozoic sea-surface-temperature evolution of the South Atlantic Ocean. *Climate of the Past*, *19*(10), 1931–1949. https://doi.org/10.5194/cp-19-1931-2023

Hoem, F. S., van den Broek, K., López-Quirós, A., van de Lagemaat, S. H., Bohaty, S. M., Hillenbrand, C. D., et al. (2024). Stepwise Oligocene–Miocene breakdown of subpolar gyres and strengthening of the Antarctic Circumpolar Current. *Journal of Micropalaeontology*, *43*(2), 497–517. https://doi.org/10.5194/jm-43-497-2024

Hudson, J. D., & Anderson, T. F. (1989). Ocean temperatures and isotopic compositions through time. *Earth and Environmental Science Transactions of the Royal Society of Edinburgh*, *80*(3–4), 183–192. https://doi.org/10.1017/s0263593300028625

Ihering, H. (1907). Les Mollusques fossiles du Tertiaire et du Cretacé Supérieur de l'Argentine. *Anales del Museo Nacional de Buenos Aires, serie 3*, *14*(7), 1–611.

Ivany, L. C., & Acosta, R. P. (2025). Approaching the Miocene climatic optimum in Patagonia (southern Argentina): Temperature seasonality and a potential role for the opening Drake Passage [Dataset]. *Zenodo*. https://doi.org/10.5281/zenodo.15256352

Ivany, L. C., & Judd, E. J. (2022). Deciphering temperature seasonality in Earth's ancient oceans. *Annual Review of Earth and Planetary Sciences*, *50*(1), 123–152. https://doi.org/10.1146/annurev-earth-032320-095156

Ivany, L. C., Lohmann, K. C., Hasiuk, F., Blake, D. B., Glass, A., Aronson, R. B., & Moody, R. M. (2008). Eocene climate record of a high southern latitude continental shelf: Seymour Island, Antarctica. *Geological Society of America Bulletin*, *120*(5–6), 659–678. https://doi.org/10.1130/b26269.1

Jones, D. S., & Quitmyer, I. R. (1996). Marking time with bivalve shells: Oxygen isotopes and season of annual increment formation. *PALAIOS*, *11*(4), 340–346. https://doi.org/10.2307/3515244

Judd, E. J., Bhattacharya, T., & Ivany, L. C. (2020). A dynamical framework for interpreting ancient sea surface temperatures. *Geophysical Research Letters*, *47*(15), e2020GL089044. https://doi.org/10.1029/2020gl089044

Judd, E. J., Ivany, L. C., DeConto, R. M., Halberstadt, A. R. W., Miklus, N. M., Junium, C. K., & Uveges, B. T. (2019). Seasonally resolved proxy data from the Antarctic Peninsula support a heterogeneous middle Eocene Southern Ocean. *Paleoceanography and Paleoclimatology*, *34*(5), 787–799. https://doi.org/10.1029/2019pa003581

Judd, E. J., Wilkinson, B. H., & Ivany, L. C. (2018). The life and time of clams: Derivation of intra-annual growth rates from high-resolution oxygen isotope profiles. *Palaeogeography, Palaeoclimatology, Palaeoecology*, *490*, 70–83. https://doi.org/10.1016/j.palaeo.2017.09.034

Kasbohm, J., & Schoene, B. (2018). Rapid eruption of the Columbia River flood basalt and correlation with the mid-Miocene climate optimum. *Science Advances*, *4*(9), eaat8223. https://doi.org/10.1126/sciadv.aat8223

Kennett, J. P. (1977). Cenozoic evolution of Antarctic glaciation, the circum-Antarctic Ocean, and their impact on global paleoceanography. *Journal of Geophysical Research*, *82*(27), 3843–3860. https://doi.org/10.1029/jc082i027p03843

Knoll, K., Landman, N. H., Cochran, J. K., Macleod, K. G., & Sessa, J. A. (2016). Microstructural preservation and the effects of diagenesis on the carbon and oxygen isotope composition of Late Cretaceous aragonitic mollusks from the Gulf Coastal Plain and the Western Interior Seaway. *American Journal of Science*, *316*(7), 591–613. https://doi.org/10.2475/07.2016.01

Lagabrielle, Y., Goddéris, Y., Donnadieu, Y., Malavieille, J., & Suarez, M. (2009). The tectonic history of Drake Passage and its possible impacts on global climate. *Earth and Planetary Science Letters*, *279*(3–4), 197–211. https://doi.org/10.1016/j.epsl.2008.12.037

Lear, C. H., Coxall, H. K., Foster, G. L., Lunt, D. J., Mawbey, E. M., Rosenthal, Y., et al. (2015). Neogene ice volume and ocean temperatures: Insights from infaunal foraminiferal Mg/Ca paleothermometry. *Paleoceanography*, *30*(11), 1437–1454. https://doi.org/10.1002/2015pa002833

Lear, C. H., Elderfield, H., & Wilson, P. A. (2000). Cenozoic deep-sea temperatures and global ice volumes from Mg/Ca in benthic foraminiferal calcite. *Science*, *287*(5451), 269–272. https://doi.org/10.1126/science.287.5451.269

Lear, C. H., Mawbey, E. M., & Rosenthal, Y. (2010). Cenozoic benthic foraminiferal Mg/Ca and Li/Ca records: Toward unlocking temperatures and saturation states. *Paleoceanography*, *25*(4). https://doi.org/10.1029/2009pa001880

Lear, C. H., Rosenthal, Y., & Slowey, N. (2002). Benthic foraminiferal Mg/Ca-paleothermometry: A revised core-top calibration. *Geochimica et Cosmochimica Acta*, *66*(19), 3375–3387. https://doi.org/10.1016/s0016-7037(02)00941-9

LeGrande, A. N., & Schmidt, G. A. (2006). Global gridded data set of the oxygen isotopic composition in seawater. *Geophysical Research Letters*, *33*(12), L12604. https://doi.org/10.1029/2006gl026011

Leutert, T. J., Modestou, S., Bernasconi, S. M., & Meckler, A. N. (2021). Southern Ocean bottom-water cooling and ice sheet expansion during the middle Miocene climate transition. *Climate of the Past*, *17*(5), 2255–2271. https://doi.org/10.5194/cp-17-2255-2021

Levy, R., Harwood, D., Florindo, F., Sangiorgi, F., Tripati, R., von Eynatten, H., et al. (2016). Antarctic ice sheet sensitivity to atmospheric CO2 variations in the early to mid-Miocene. *Proceedings of the National Academy of Sciences*, *113*(13), 3453–3458. https://doi.org/10.1073/pnas.1516030113

Lowenstein, T. K., & Hönisch, B. (2012). The use of Mg/Ca as a seawater temperature proxy. *Paleontological Society Papers*, *18*, 85–100. https://doi.org/10.1017/s1089332600002564

Lunt, D. J., Farnsworth, A., Loptson, C., Foster, G. L., Markwick, P., O'Brien, C. L., et al. (2016). Palaeogeographic controls on climate and proxy interpretation. *Climate of the Past*, *12*(5), 1181–1198. https://doi.org/10.5194/cp-12-1181-2016

Lunt, D. J., Otto-Bliesner, B. L., Brierley, C., Haywood, A., Inglis, G. N., Izumi, K., et al. (2024). Paleoclimate data provide constraints on climate models' large-scale response to past CO_2 changes. *Communications Earth & Environment*, *5*(1), 419. https://doi.org/10.1038/s43247-024-01531-3

Lyle, M., Gibbs, S., Moore, T. C., & Rea, D. K. (2007). Late Oligocene initiation of the Antarctic circumpolar current: Evidence from the South Pacific. *Geology*, *35*(8), 691–694. https://doi.org/10.1130/g23806a.1

Malumián, N., & Náñez, C. (1991). *Paleogeografía del Terciario medio del cono sur: avance de aguas antárticas.* 6 Congreso Geológico Chileno, Resúmenes Expandidos (pp. 847–851). Servicio Nacional de Geología y Minería, Viña del Mar.

Malumián, N., & Náñez, C. (2011). The late Cretaceous–Cenozoic transgressions in Patagonia and the Fuegian Andes: Foraminifera, palaeoecology, and palaeogeography. *Biological Journal of the Linnean Society*, *103*(2), 269–288. https://doi.org/10.1111/j.1095-8312.2011.01649.x

Martínez, S. A., & del Río, C. J. (2002a). Late Miocene molluscs from the southwestern Atlantic Ocean (Argentina and Uruguay): A paleobiogeographic analysis. *Palaeogeography, Palaeoecology and Palaeoclimatology*, *188*(3–4), 167–187. https://doi.org/10.1016/S0031-0182(02)00551-5

Martínez, S. A., & del Río, C. J. (2002b). Las provincias malacologicas Miocenas y recientes del Atlántico sudoccidental. *Anales de Biologia*, *24*, 121–130.

Matthews, K. J., Maloney, K. T., Zahirovic, S., Williams, S. E., Seton, M., & Müller, R. D. (2016). Global plate boundary evolution and kinematics since the late Paleozoic. *Global and Planetary Change*, *146*, 226–250. https://doi.org/10.1016/j.gloplacha.2016.10.002

McKay, R., Cockrell, J., Shevenell, A. E., Laberg, J. S., Burns, J., the IODP Expedition 374 Science Team, et al. (2024). Miocene ice sheet dynamics and sediment deposition in the central Ross Sea, Antarctica. *Geological Society of America Bulletin*, *137*(3–4), 1267–1291. https://doi.org/10.1130/B37613.1

Meckler, A. N., Sexton, P. F., Piasecki, A. M., Leutert, T. J., Marquardt, J., Ziegler, M., et al. (2022). Cenozoic evolution of deep ocean temperature from clumped isotope thermometry. *Science*, *377*(6601), 86–90. https://doi.org/10.1126/science.abk0604

Modestou, S. E., Leutert, T. J., Fernandez, A., Lear, C. H., & Meckler, A. N. (2020). Warm middle Miocene Indian Ocean bottom water temperatures: Comparison of clumped isotope and Mg/Ca-based estimates. *Paleoceanography and Paleoclimatology*, *35*(11), e2020PA003927. https://doi.org/10.1029/2020pa003927

Náñez, C., Quattrocchio, M., & Ruiz, L. (2009). Palinología y micropaleontología de las Formaciones San Julián y Monte León (Oligoceno–Mioceno temprano) en el subsuelo de cabo Curioso, provincia de Santa Cruz, Argentina. *Ameghiniana*, *46*, 669–693.

Nicol, D. (1950). Recent species of the prionodont pelecypod *Cucullaea*. *Journal of the Washington Academy of Sciences*, *40*, 338–343.

Nirenberg, J. E., & Herbert, T. D. (2025). North Pacific warmth synchronous with the Miocene climatic optimum. *Geology*, *53*(2), 145–149. https://doi.org/10.1130/g52432.1

Parras, A., & Cuitiño, J. (2018). The stratigraphic and paleoenvironmental significance of the regressive Monte Observación Member, early Miocene of the austral basin. *Latin American Journal of Sedimentology and Basin Analysis*, *25*(2), 25–47.

Parras, A., & Cuitiño, J. (2021). Revised chrono and lithostratigraphy for the Oligocene- Miocene *Patagoniense* marine deposits in Patagonia: Implications for stratigraphic cycles, paleogeography, and major drivers. *Journal of South American Earth Sciences*, *110*, 103327. https://doi.org/10.1016/j.jsames.2021.103327

Parras, A., Dix, G. R., & Griffin, M. (2012). Sr-isotope chronostratigraphy of Paleogene-Neogene marine deposits: Austral Basin, southern Patagonia (Argentina). *Journal of South American Earth Sciences*, *37*, 122–135. https://doi.org/10.1016/j.jsames.2012.02.007

Parras, A., & Griffin, M. (2009). Darwin's great patagonian Tertiary Formation at the mouth of the río Santa Cruz: A reappraisal. In B. Aguirre-Urreta, M. Griffin, & V. A. Ramos (Eds.), *Darwin in Argentina. Revista de la Asociación Geológica Argentina* (Vol. 64, pp. 70–82).

Parras, A., Guerstein, R. G., Pérez Panera, J. P., Griffin, M., Náñez, C., Cusminsky, G., & Quiroga, A. (2020). Integrated stratigraphy and paleontology of the lower Miocene Monte León Formation, southeastern Patagonia, Argentina: Unraveling paleoenvironmental changes and factors controlling sedimentation. *Palaeogeography, Palaeoclimatology, Palaeoecology*, *556*, 1–22. https://doi.org/10.1016/j.palaeo.2020.109701

Passchier, S., Browne, G., Field, B., Fielding, C. R., Krissek, L. A., Panter, K., et al. (2011). Early and Middle Miocene Antarctic glacial history from the sedimentary facies distribution in the AND-2A drill hole, Ross Sea, Antarctica. *Bulletin of the Geological Society of America*, *123*(11–12), 2352–2365. https://doi.org/10.1130/b30334.1

Pérez, L. F., Hernández-Molina, F. J., Lodolo, E., Bohoyo, F., Galindo-Zaldívar, J., & Maldonado, A. (2019). Oceanographic and climatic consequences of the tectonic evolution of the southern scotia sea basins, Antarctica. *Earth-Science Reviews*, *198*, 102922. https://doi.org/10.1016/j.earscirev.2019.102922

Perkins, M. E., Fleagle, J. G., Heizler, M. T., Nash, B., Bown, T. M., Tauber, A. A., & Dozo, M. T. (2012). Tephrochronology of the Miocene Santa Cruz and pinturas formations, Argentina. In S. F. Vizcaíno, R. F. Kay, & M. S. Bargo (Eds.), *Early Miocene Paleobiology in Patagonia: High-Latitude Paleocommunities of the Santa Cruz Formation* (pp. 23–40). Cambridge University Press.

Pineda-Salgado, G., Parras, A., & Griffin, M. (2022). Taphonomic analysis of fossil concentrations from the Monte León Formation (lower Miocene), Santa Cruz Province, Argentina. *Journal of South American Earth Sciences*, *114*, 103671. https://doi.org/10.1016/j.jsames.2021.103671

Ring, S. J., Mutz, S. G., & Ehlers, T. A. (2022). Cenozoic proxy constraints on Earth system sensitivity to greenhouse gases. *Paleoceanography and Paleoclimatology*, *37*(12), e2021PA004364. https://doi.org/10.1029/2021pa004364

Rohling, E. J., Foster, G. L., Gernon, T. M., Grant, K. M., Heslop, D., Hibbert, F. D., et al. (2022). Comparison and synthesis of sea-level and deep-sea temperature variations over the past 40 million years. *Reviews of Geophysics*, *60*(4), e2022RG000775. https://doi.org/10.1029/2022rg000775

Santelli, M. B., & del Río, C. J. (2019a). The Neogene Chlamydini Teppner, 1922 of Patagonia (Argentina): *Zygochlamys* Ihering, 1907 and three new endemic genera. *Journal of Paleontology*, *93*, 312–336. https://doi.org/10.1017/jpa.2018.75

Santelli, M. B., & del Río, C. J. (2019b). New Neogene taxa of the tribe Chlamydini Teppner, 1922 (Pectinidae, Bivalvia) of southern South America. *Journal of Paleontology*, *93*(6), 1088–1104. https://doi.org/10.1017/jpa.2019.50

Sauermilch, I., Whittaker, J. M., Klocker, A., Munday, D. R., Hochmuth, K., Bijl, P. K., & LaCasce, J. H. (2021). Gateway-driven weakening of ocean gyres leads to Southern Ocean cooling. *Nature Communications*, *12*(1), 6465. https://doi.org/10.1038/s41467-021-26658-1

Sibert, E. C., & Rubin, L. D. (2021). An early Miocene extinction in pelagic sharks. *Science*, *372*(6546), 1105–1107. https://doi.org/10.1126/science.aaz3549

Sowerby, R. (1846). Description of the Tertiary fossils shells from South America. In Ch. Darwin (Ed.), *Geological Observations on the volcanics Islands and parts of South America visited during the voyage of H.M.S. Beagle* (p. 548).

Steinthorsdottir, M., Coxall, H. K., De Boer, A. M., Huber, M., Barbolini, N., Bradshaw, C. D., et al. (2021). The Miocene: The future of the past. *Paleoceanography and Paleoclimatology*, *36*(4), e2020PA004037. https://doi.org/10.1029/2020pa004037

Tierney, J. E., Poulsen, C. J., Montañez, I., Bhattacharya, T., Feng, R., Ford, H. L., et al. (2020). Past climates inform our future. *Science*, *370*(6517), eaay3701. https://doi.org/10.1126/science.aay3701

Toumoulin, A., Donnadieu, Y., Ladant, J. B., Batenburg, S. J., Poblete, F., & Dupont-Nivet, G. (2020). Quantifying the effect of the Drake passage opening on the Eocene Ocean. *Paleoceanography and Paleoclimatology*, *35*(8), e2020PA003889. https://doi.org/10.1029/2020pa003889

Unland, E., Miramontes, E., Spiess, V., Bozzano, G., Kasten, S., & Schwenk, T. (2024). Evolution of a buried moat–drift system in the Ewing Terrace uncovering highly dynamic bottom currents at the Argentine margin from the early Oligocene to middle Miocene. *Journal of Sedimentary Research*, *94*(6), 784–798. https://doi.org/10.2110/jsr.2024.030

van de Lagemaat, S. H., Swart, M. L., Vaes, B., Kosters, M. E., Boschman, L. M., Burton-Johnson, A., et al. (2021). Subduction initiation in the Scotia Sea region and opening of the Drake Passage: When and why? *Earth-Science Reviews*, *215*, 103551. https://doi.org/10.1016/j.earscirev.2021.103551

van Hinsbergen, D. J., De Groot, L. V., van Schaik, S. J., Spakman, W., Bijl, P. K., Sluijs, A., et al. (2015). A paleolatitude calculator for paleoclimate studies. *PLoS One*, *10*(6), e0126946. https://doi.org/10.1371/journal.pone.0126946

Vincze, M., Bozóki, T., Herein, M., Borcia, I. D., Harlander, U., Horicsányi, A., et al. (2021). The Drake Passage opening from an experimental fluid dynamics point of view. *Scientific Reports*, *11*(1), 19951. https://doi.org/10.1038/s41598-021-99123-0

von der Heydt, A., & Dijkstra, H. A. (2006). Effect of ocean gateways on the global ocean circulation in the late Oligocene and early Miocene. *Paleoceanography*, *21*(1), PA1011. https://doi.org/10.1029/2005pa001149

Wainer, I., Gent, P., & Goni, G. (2000). Annual cycle of the Brazil-Malvinas confluence region in the National center for atmospheric Research climate system model. *Journal of Geophysical Research*, *105*(C11), 26167–26177. https://doi.org/10.1029/1999JC000134

Westerhold, T., Marwan, N., Drury, A. J., Liebrand, D., Agnini, C., Anagnostou, E., et al. (2020). An astronomically dated record of Earth's climate and its predictability over the last 66 million years. *Science*, *369*(6509), 1383–1387. https://doi.org/10.1126/science.aba6853

Wilkinson, B. H., & Ivany, L. C. (2002). Paleoclimatic inference from stable isotope profiles of accretionary biogenic hardparts–a quantitative approach to the evaluation of incomplete data. *Palaeogeography, Palaeoclimatology, Palaeoecology*, *185*(1–2), 95–114. https://doi.org/10.1016/s0031-0182(02)00279-1

Yang, S., Galbraith, E., & Palter, J. (2014). Coupled climate impacts of the Drake Passage and the Panama Seaway. *Climate Dynamics*, *43*(1–2), 37–52. https://doi.org/10.1007/s00382-013-1809-6

Zachos, J. C., Stott, L. D., & Lohmann, K. C. (1994). Evolution of early Cenozoic marine temperatures. *Paleoceanography*, *9*(2), 353–387. https://doi.org/10.1029/93pa03266

Zeebe, R. E. (2001). Seawater pH and isotopic paleotemperatures of Cretaceous oceans. *Palaeogeography, Palaeoclimatology, Palaeoecology*, *170*(1–2), 49–57. https://doi.org/10.1016/s0031-0182(01)00226-7